



## Holocene glacier activity reconstructed from proglacial lake Gjøavatnet on Amsterdamøya, NW Svalbard



Gregory A. de Wet <sup>a,\*</sup>, Nicholas L. Balascio <sup>b</sup>, William J. D'Andrea <sup>c</sup>, Jostein Bakke <sup>d</sup>, Raymond S. Bradley <sup>a</sup>, Bianca Perren <sup>e</sup>

<sup>a</sup> Department of Geosciences, University of Massachusetts Amherst, Amherst, MA, 01003, USA

<sup>b</sup> Department of Geology, College of William & Mary, Williamsburg, VA, 23187, USA

<sup>c</sup> Lamont-Doherty Earth Observatory of Columbia University, Palisades, NY, 10964, USA

<sup>d</sup> Department of Earth Science, University of Bergen, Bergen, 5007, Norway

<sup>e</sup> British Antarctic Survey, Cambridge, CB3 0ET, United Kingdom

### ARTICLE INFO

#### Article history:

Received 9 July 2016

Received in revised form

15 March 2017

Accepted 20 March 2017

Available online 29 April 2017

#### Keywords:

Holocene paleoclimate

Svalbard

Lake sediments

Glaciers

Fram strait

Freshwater forcing

### ABSTRACT

Well-dated and highly resolved paleoclimate records from high latitudes allow for a better understanding of past climate change. Lake sediments are excellent archives of environmental change, and can record processes occurring within the catchment, such as the growth or demise of an upstream glacier. Here we present a Holocene-length, multi-proxy lake sediment record from proglacial lake Gjøavatnet on the island of Amsterdamøya, northwest Svalbard. Today, Gjøavatnet receives meltwater from the Annabreen glacier and contains a record of changes in glacier activity linked to regional climate conditions. We measured changes in organic matter content, dry bulk density, bulk carbon isotopes, elemental concentrations via Itrax core-scanning, and diatom community composition to reconstruct variability in glacier extent back through time. Our reconstruction indicates that glacially derived sedimentation in the lake decreased markedly at ~11.1 cal kyr BP, although a glacier likely persisted in the catchment until ~8.4 cal kyr BP. During the mid-Holocene (~8.4–1.0 cal kyr BP) there was significantly limited glacial influence in the catchment and enhanced deposition of organic-rich sediment in the lake. The deposition of organic rich sediments during this time was interrupted by at least three multi-centennial intervals of reduced organic matter accumulation (~5.9–5.0, 2.7–2.0, and 1.7–1.5 cal kyr BP). Considering our chronological information and a sedimentological comparison with intervals of enhanced glacier input, we interpret these intervals not as glacial advances, but rather as cold/dry episodes that inhibited organic matter production in the lake and surrounding catchment. At ~1.0 cal kyr BP, input of glacially derived sediment to Gjøavatnet abruptly increased, representing the rapid expansion of the Annabreen glacier.

© 2017 Elsevier Ltd. All rights reserved.

### 1. Introduction

Reliable and highly resolved paleoclimate reconstructions are necessary in order to better contextualize recent and predicted climate change (Kaplan and Wolfe, 2006), especially from high latitudes where these changes are expected to be greatest (Callaghan et al., 2010; Serreze and Barry, 2011; Stocker et al., 2013). Glaciers and small ice caps respond rapidly to climate variations, but direct evidence for past changes in ice extent in remote areas is

temporally and spatially limited. The Holocene Epoch (past ~11.7 thousand calendar years before present (cal kyr BP)) provides important context to understand Arctic climate dynamics because atmospheric and ocean circulation patterns were similar to their current configuration and natural insolation forcing caused widespread environmental change without the overprint of significant anthropogenic influence (until recent decades) (Johnsen et al., 2001; Kaufman et al., 2004; Mayewski et al., 2004). Broad scale Arctic climate throughout this interval is understood to have been characterized by early Holocene warmth that progressively transitioned toward a colder late Holocene (i.e., the Neoglacial), driven mainly by declining high latitude summer insolation (Laskar et al., 2004; Miller et al., 2010; Briner et al., 2016). Superimposed on this

\* Corresponding author.

E-mail address: [gdewet@geo.umass.edu](mailto:gdewet@geo.umass.edu) (G.A. de Wet).

trend are spatial heterogeneities linked to the decaying Northern Hemisphere ice sheets and associated meltwater pulses (e.g. Sejrup et al., 2016). High-resolution paleoclimate records are important to better examine the timing, expression, and magnitude of Holocene climate change throughout the Arctic.

The Svalbard archipelago is uniquely situated at the intersection between the northern North Atlantic and the Arctic Ocean basins (Fig. 1). Near Svalbard, warm Atlantic Water transported via the West Spitsbergen Current (WSC) mixes with cold, less saline water from the Arctic Ocean. Atmospheric conditions are influenced by the relative influence of cold, polar-derived air masses from the north and east and warmer subpolar maritime air masses from the south and southwest (Førland et al., 2011). The relative locations of these important boundaries, along with associated sea ice feedbacks, has been shown to vary throughout the Holocene and influence climate in Svalbard (e.g. Müller et al., 2012; Werner et al., 2013, 2015; Rasmussen et al., 2014).

Broadly, evidence from marine records near Svalbard and in the northern North Atlantic suggests a warm early Holocene period (~11–8 kyr BP), characterized by an increased flux of Atlantic water to high latitudes (Sarnthein et al., 2003; Hald et al., 2004, 2007; Ślubowska et al., 2005; Forwick and Vorren, 2009; Skirbekk et al., 2010; Risebækken et al., 2011; Müller et al., 2012; Werner et al., 2013, 2015; Aagaard-Sørensen et al., 2014; Rasmussen et al., 2014). The transition to cooler (Neoglacial) conditions during the middle Holocene is not well constrained, with some records suggesting cooling began as early 8.8 cal kyr BP (e.g. Hald et al., 2004), while others point to cooling beginning ~6 kyr BP (e.g. Rasmussen et al., 2014). Oceanic conditions near Svalbard during the late Holocene are generally characterized by cold temperatures

overprinted by fluctuations linked to changes in the advection of warm Atlantic Water in the WSC (e.g. Ślubowska et al., 2005; Werner et al., 2013; Aagaard-Sørensen et al., 2014; Berben et al., 2014).

While there has been an increase in the number of terrestrial Holocene paleoclimate studies from Svalbard in recent years (e.g. D'Andrea et al., 2012; Reusche et al., 2014; Røthe et al., 2015; van der Bilt et al., 2015; van der Bilt et al., 2016; Gjerde et al., in press; Balascio et al., in press), this region generally lacks continuous, well-dated paleoenvironmental reconstructions. Retreat of the Barents Sea Ice Sheet had begun during the end of the Pleistocene (~20–14 cal kyr BP) (Gjermundsen et al., 2013; Hormes et al., 2013; Ingólfsson and Landvik, 2013), and numerous records suggest many smaller glaciers in Svalbard retreated or completely melted during the early Holocene (Svendsen and Mangerud, 1997; Snyder et al., 2000; Reusche et al., 2014; Røthe et al., 2015; van der Bilt et al., 2015). The timing of late-Holocene glacial re-advance however, remains poorly constrained; some studies suggest glaciers advanced ~3–4 cal kyr BP (Svendsen and Mangerud, 1997; Reusche et al., 2014; Røthe et al., 2015), while others point to a later advance closer to 1 cal kyr BP (Snyder et al., 2000; Humlum et al., 2005; van der Bilt et al., 2015).

Here we present a glacier reconstruction from proglacial lake Gjøavatnet on the island of Amsterdamøya in NW Svalbard spanning the Holocene (Fig. 1). The objective of this study is to reconstruct the history of the upstream Annabreen glacier (Fig. 1) towards a better understanding of Holocene climate change in the region. The maritime climate of Amsterdamøya, and the presence of a glacier in the Gjøavatnet catchment, makes this record valuable for addressing questions about past climate variations in the High

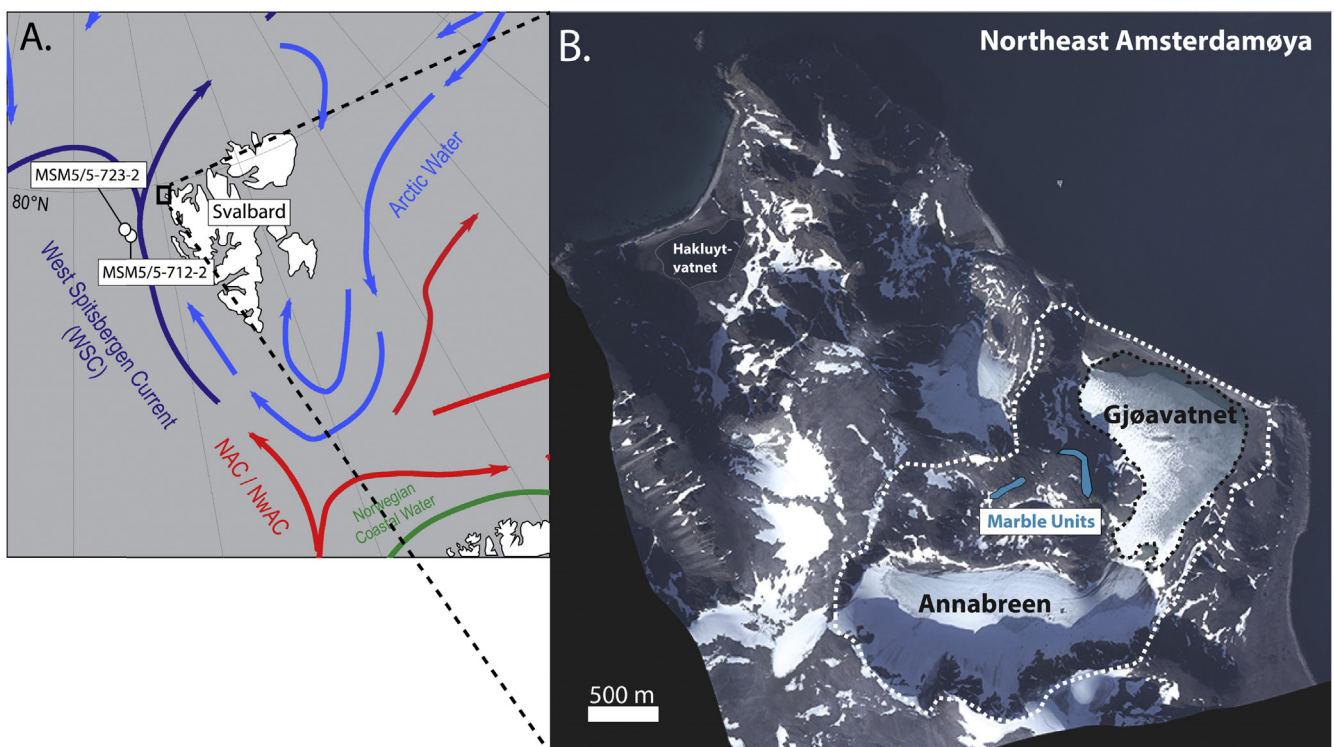


**Fig. 1.** A) Map of Svalbard and surrounding surface currents as well as locations of marine sediment cores MSM5/5-723-2 and MSM5/5-712-2 (Werner et al., 2013, 2015); B) Aerial image of island of Amsterdamøya with Annabreen glacier and Gjøavatnet lake (this study) and Halkuytuvatnet lake (Gjerde et al., in press) labeled. Blue polygons represent the approximate locations of marble outcrops (Ohta et al., 2007). Dashed white line denotes approximate catchment of Gjøavatnet. (For interpretation of the references to colour in this figure legend, the reader is referred to the web version of this article.)

Arctic North Atlantic. Our record suggests that Annabreen disappeared or was dramatically reduced in size by ~8.4 cal kyr BP. During the interval 8.4–1 cal kyr BP, sedimentation in the lake was marked by higher amounts of organic material accumulation, but was punctuated by multi-centennial-length periods with relatively lower organic matter content. A return to minerogenic sedimentation at 1 cal kyr BP is interpreted to represent the re-advance of Annabreen at that time.

## 2. Regional setting

Svalbard's climate is characterized by highly variable temperatures and low average annual precipitation. A meteorological station at Ny-Ålesund, ~95 km south of Amsterdamøya, recorded average annual temperatures of  $-5.2^{\circ}\text{C}$  over the period 1981–2010, though average temperatures of individual years ranged from  $-12^{\circ}\text{C}$  to  $3.8^{\circ}\text{C}$  (Førland et al., 2011). The average annual precipitation at Ny-Ålesund is 427 mm (Førland et al., 2011), with the majority of moisture sourced from the south/southwest and occurring during the fall and winter months (Førland et al., 2011). The dry nature of this environment suggests that relatively small changes in the precipitation budget could play a large role in the mass balance of local glaciers. There is a positive relationship between temperature and precipitation in all seasons (Førland et al., 2011).

### 2.1. Study site

Lake Gjøavatnet ( $79^{\circ}46'00''\text{N}$ ,  $10^{\circ}51'45''\text{E}$ , 2 m a.s.l.) is a small proglacial lake on the eastern coast of Amsterdamøya, Svalbard (Fig. 1). The lake catchment contains a steep-sided cirque (area of  $\sim 2.8 \text{ km}^2$ ), marked by the presence of the Annabreen glacier (surface area of  $0.87 \text{ km}^2$ ), which currently terminates in the southwest corner of the lake. The limited vegetation in the catchment is characterized as northern Arctic tundra (Birks et al., 2004). Gjøavatnet itself has an area of  $\sim 0.52 \text{ km}^2$  and has a maximum depth of  $\sim 15 \text{ m}$ . The lake is separated from the ocean by a narrow ( $\sim 30 \text{ m}$  wide) strip of bedrock (Hjelle and Ohta, 1974; Ohta et al., 2007), which is currently covered with large numbers of smoothed boulders and driftwood (Fig. 1). There has been no net postglacial uplift relative to sea level in the immediate region during the Holocene (Forman, 1990; Landvik et al., 1998, 2003). The surrounding bedrock is comprised mainly of Mesoproterozoic banded gneiss and migmatite of the Smeerenburgfjorden Complex containing small outcrops of marble with skarn mineralization in the northwestern part of the catchment (blue outlines in Fig. 1) (Hjelle and Ohta, 1974; Ohta et al., 2007).

## 3. Methods

### 3.1. Fieldwork and lake coring

Prior to coring, Gjøavatnet was surveyed using ground penetrating radar (GPR) as well as a Lowrance sonar bathymetric device to determine lake bottom bathymetry and soft sediment distribution (Fig. 2). GPR profiles were collected using a Mala RAMAC GPR unit with a 50 MHZ antenna.

Five sediment cores were collected from Gjøavatnet in the summer of 2014; 2 piston cores (GJP-01-14; 210 cm in length, and GJP-02-14; 82 cm), and 3 gravity/surface cores (GJD-01-14; 39 cm, GJD-02-14; 46 cm, and GJD-03-14; 42 cm) (Table 1) (see Fig. 2 for coring locations). Surface cores were collected using a Uwitec surface corer. Piston cores were collected using a percussion piston coring device and were hammered until refusal to ensure maximum sediment recovery. GJP-01-14 was cut into two sections

in the field (1 of 2: 135.5 cm long, 2 of 2: 71 cm long) to allow for transport. The sediment cores were then shipped back to the University of Bergen for splitting and analysis.

### 3.2. Composite sediment record

A composite sediment record was created based mainly on piston core GJP-01-14, which was collected from the deepest part of the lake (Fig. 2) and is the longest core retrieved from Gjøavatnet (Fig. 3). Comparison of both visual stratigraphy and proxy data between piston core GJP-01-14 and surface cores GJD-01-14 and GJD-02-14 (recovered from the same basin) reveal that only 2.5 cm of sediment were lost from the upper part of the GJP-01-14 during piston coring. The basal sediment in both piston cores (GJP-01-14 and GJP-02-14) is comprised of diamict, interpreted as glacial till, suggesting the entire Holocene record was recovered (Fig. 3). To achieve the highest resolution record possible we focused our investigation on the GJP-01-14 core (206.5 cm length). Results from this core form the basis of most of our interpretations.

### 3.3. Laboratory analyses

Cores were split and imaged at the University of Bergen prior to analysis. All five cores were analyzed for surface magnetic susceptibility (MS) at 0.5 cm resolution using a Bartington MS2E point sensor. The cores were also analyzed using an ITRAX X-ray fluorescence (XRF) core scanner located at EARTHLAB, University of Bergen, to determine elemental concentrations. Scans were carried out using a molybdenum (Mo) tube with a downcore resolution of 200  $\mu\text{m}$ . The voltage and current were set to 30 kV and 45 mA respectively, with an XRF count time of 10 s. For GJP-01-14, Itrax core scanning data were not collected below 167 cm depth because the sediment surface was too uneven for the instrument to accommodate.

GJP-01-14 was sub-sampled at 0.5 cm intervals for weight loss-on-ignition (LOI), dry bulk density (DBD), and water content (WC) ( $n = 335$ ) (after Dean, 1974; Heiri et al., 2001). A syringe was used to ensure a constant 1  $\text{cm}^3$  of sediment was removed. The sediment below  $\sim 167 \text{ cm}$  in GJP-01-14 was either too stiff to properly remove the necessary volume of sediment for accurate LOI and DBD analysis or was simply composed of large clasts, making the analyses impossible. Accordingly, the majority of our proxy data (and associated figures) do not include data from the bottom  $\sim 40 \text{ cm}$  of the GJP-01-14 core.

Macrofossils for radiocarbon dating were removed and sent to the Poznan Radiocarbon Laboratory in Poland for analysis (Table 2).  $\delta^{13}\text{C}$  values of bulk sediment ( $n = 50$ ) were measured at the Lamont Doherty Earth Observatory using a Costech elemental combustion system (EA) coupled to a Delta V Plus IRMS (Thermo). A two-point isotope calibration curve was constructed using standards USGS40 and USGS41 to place measured values on the VPDB scale. A third standard (USGS24) was run during the period of data acquisition to evaluate the accuracy of measurement.

Eight samples were chosen for diatom taxonomic analysis from 121.5, 135.5, 137, 149.5, 161.5, 163.5, 164.5, and 165.5 cm composite depth in GJP-01-14 to evaluate the possibility of early Holocene marine incursions and to characterize lacustrine conditions. Diatoms were isolated from the sediments using standard oxidative techniques modified from Renberg (1990) and mounted on glass coverslips using Naphrax mounting medium. At least 300 diatom samples were identified from each slide at 1000 $\times$  under oil immersion and identified using predominantly Arctic diatom floras (e.g. Antoniades, 2008).

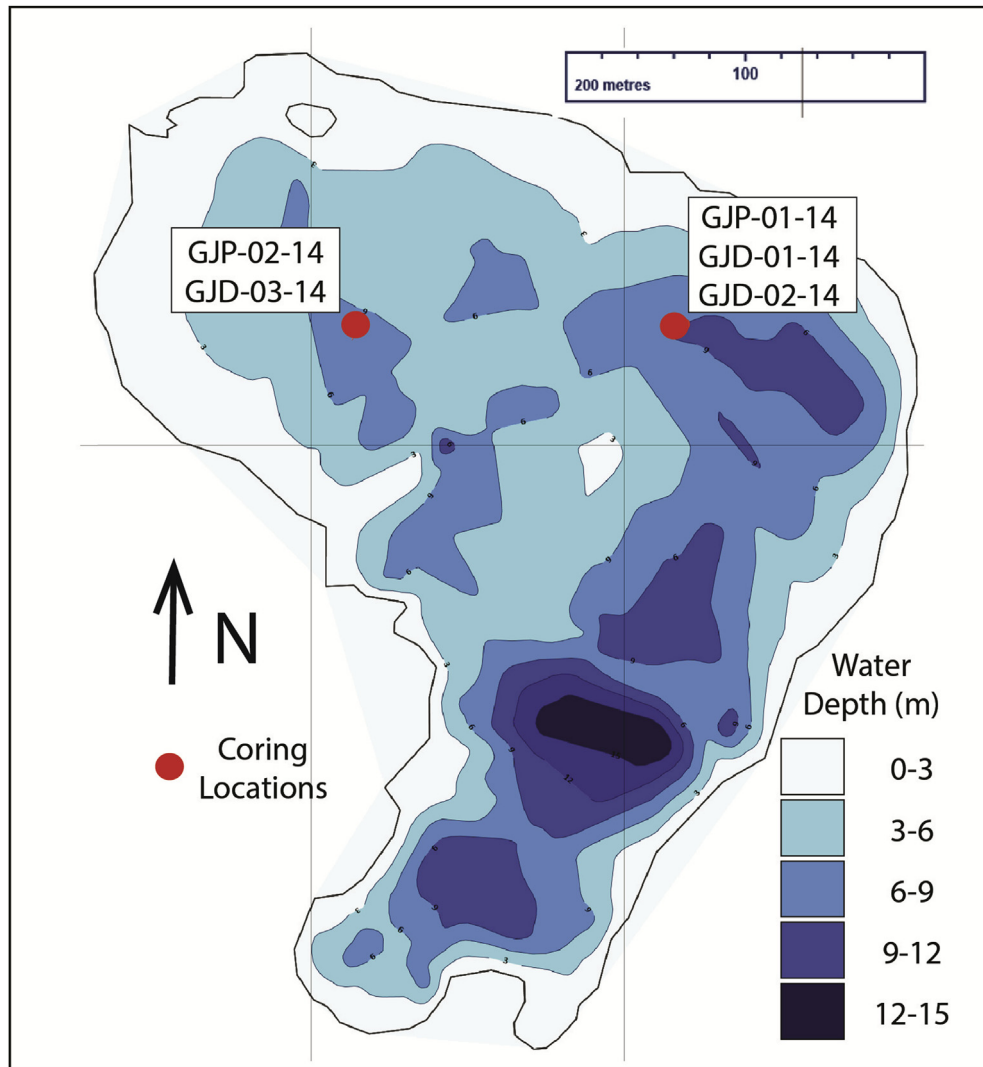


**Fig. 2.** Bathymetric map of Gjøavatnet with coring sites noted by red circles. Our investigation focused mainly on core GJP-01-14 from eastern basin. (For interpretation of the references to colour in this figure legend, the reader is referred to the web version of this article.)

**Table 1**  
Sediment cores collected from Gjøavatnet.

Core Name	GJP-01-14	GJP-02-14	GJD-01-14	GJD-02-14	GJD-03-14
Core Type	Piston	Piston	Surface/Gravity	Surface/Gravity	Surface/Gravity
Core Length (cm)	206.5	95	30	43	42

### 3.4. Statistical and multivariate analyses

Principal component analysis (PCA) and computation of correlation coefficients were carried out on 10 measured proxies using Matlab software for Windows. This included 9 geochemical element counts (Ti, K, Ca, Rb, Sr, Fe, Mn, Si, Al) from the Itrax core scanner as well as %LOI. These elements were selected based on their high signal response on the Itrax (counts per second generally  $>100$ ), their prevalence in siliciclastic sediments, and previous studies that have identified them as useful for reconstructing mineralogenic input from bedrock erosion (Bakke et al., 2013; Balascio et al., 2015; Røthe et al., 2015). Itrax data were smoothed using a 24 pt running mean and resampled at 0.5 cm intervals to achieve comparable resolution to the LOI data. All datasets were

also log-transformed prior to analysis.

## 4. Results and interpretations

### 4.1. Chronology

The chronology of the composite sedimentary record is based on 13 radiocarbon dates of organic macrofossils taken from the GJP-01-14 core (Table 2). An age model was created using the Clam age modeling package (Blaauw, 2010) for the open-source software R (v. 3.0.1; R Development Core Team, 2012) (Fig. 4). A smooth spline function was used to create the age model, with a default smoothing value of 0.3 applied. Radiocarbon dates were calibrated using the terrestrial northern hemisphere Intcal13.14C curve

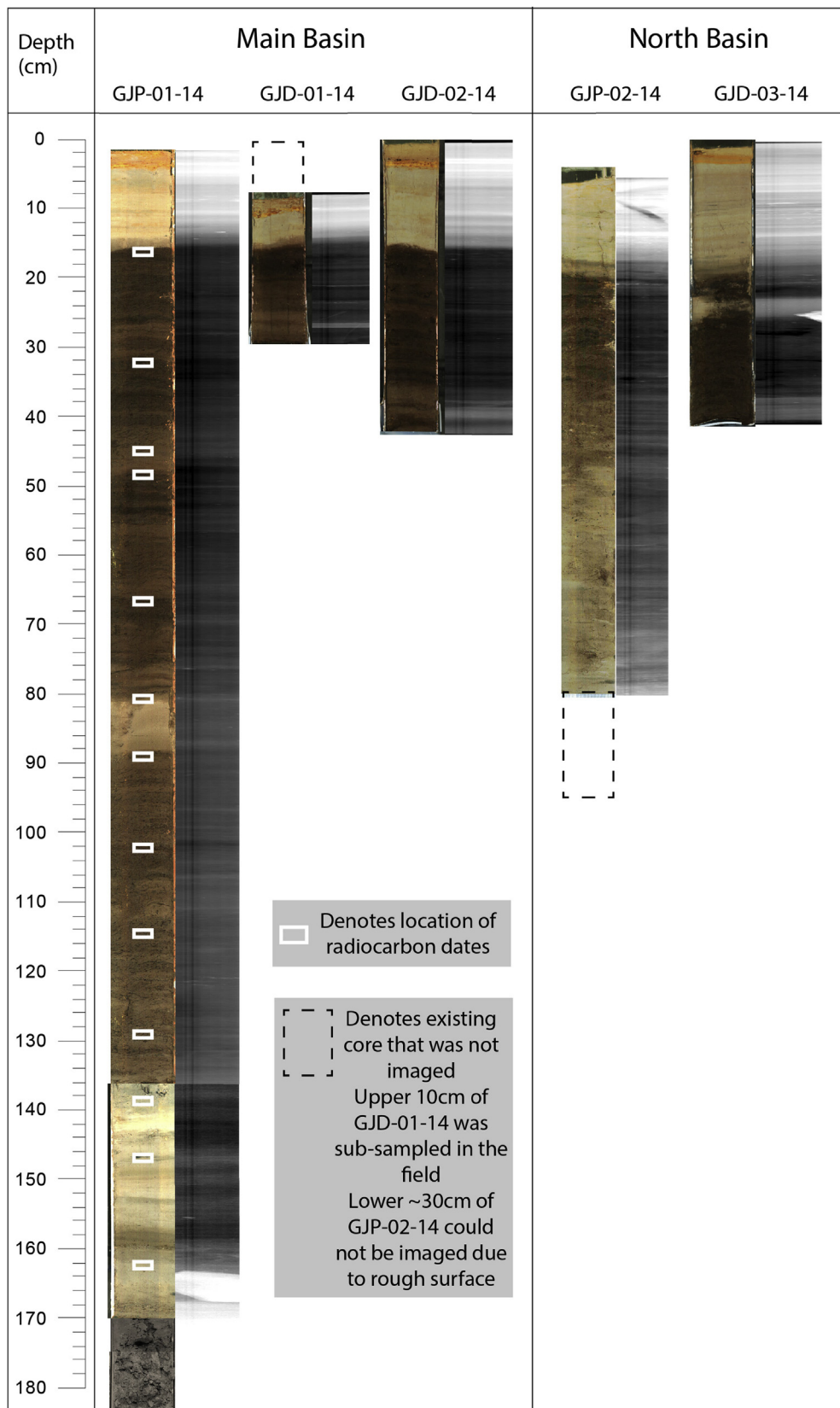


**Fig. 3.** Line-scan images and x-radiographs of all cores collected from Gjøavatnet. GJP-01-14 was the focus of this investigation. Depth of radiocarbon dates are denoted with white rectangles. Dashed black lines represent existing core that could not be imaged. Lighter shades in x-radiographs represent denser material. Note that color difference in lowest portion of GJP-01-14 (section from ~170 to 180 cm) is due to different lighting during imaging.

**Table 2**

Radiocarbon results from macrofossils taken from GJP-01-14 core.

Core	Composite Depth (cm)	Sample Material	Sample Mass (mg)	mg Carbon	<sup>14</sup> C Age	Error +/- (1σ)	Calibrated Age ±2 sigma	Δ <sup>13</sup> C % VPDB
GJP-01-14 1of2	16	Plant Remains	4.2	0.8	1125	30	960–1172	-23
GJP-01-14 1of2	32	Plant Remains	9.1	0.8	1795	35	1619–1819	-22.4
GJP-01-14 1of2	44.5	Plant Remains	4.4	0.8	2175	35	2066–2312	-20.5
GJP-01-14 1of2	48.5	Plant Remains	7.8	0.7	2685	30	2753–2846	-24
GJP-01-14 1of2	66	Plant Remains	11.6	1.02	3530	35	3702–3895	-22.8
GJP-01-14 1of2	80.5	Plant Remains	2.2	0.5	4230	40	4628–4861	-24.1
GJP-01-14 1of2	88	Plant Remains	6.9	0.5	5350	50	6002–6084	-24.4
GJP-01-14 1of2	102	Plant Remains	8.7	0.6	5860	40	6563–6778	-27.7
GJP-01-14 1of2	114	Plant Remains	6.2	1.01	6520	50	7323–7556	-22.4
GJP-01-14 1of2	129	Plant Remains	14.2	1.35	7060	50	7789–7976	-25.5
GJP-01-14 2of2	138.5	Plant Remains	3.9	0.51	7590	40	8343–8448	-26.8
GJP-01-14 2of2	146.5	Plant Remains	3.6	Not Reported	8550	30	9494–9547	-26.1
GJP-01-14 2of2	162.5	Plant Remains	2.9	Not Reported	9690	40	10,827–11,217	Not Reported

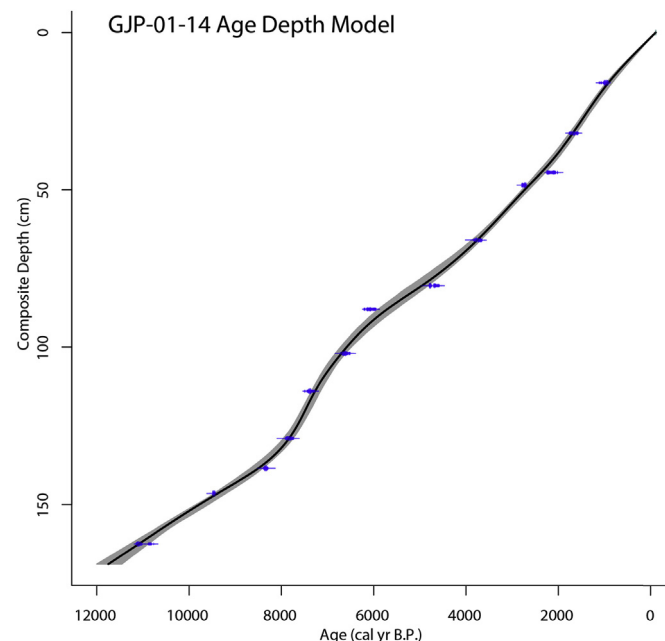


**Fig. 4.** Age depth relationship for GJP-01-14 core created in using the Clam modeling package (Blaauw, 2010) for software R (v. 3.0.1; R Development Core Team, 2012) with 95% confidence intervals for individual radiocarbon dates in blue. (For interpretation of the references to colour in this figure legend, the reader is referred to the web version of this article.)

(Reimer et al., 2013). Calculated sedimentation rates in Gjøavatnet using this age model vary from a maximum of ~29.8 cm/kyr to a minimum of ~8.6 cm/kyr with an average value of 14.7 cm/kyr. We also created an age model using the same parameters but with a linear interpolation between data points instead of a smooth spline. We only use the linear interpolation-based age model as an illustrative tool to highlight differences in sedimentation rate throughout the core, and do not use it for any of our paleoclimate interpretations. We note that age estimates below a depth of 162.5 cm (11,140 cal yr BP calibrated age) are based on extrapolation of the age model and therefore have unconstrained uncertainty. This impacts only a small portion of our proxy data, which extends to ~167 cm, but does affect our ability to accurately date the onset of lacustrine sedimentation in Gjøavatnet.

#### 4.2. Multivariate analysis

Calculated correlation coefficients for each of XRF-based

elemental abundance datasets reveal that most of the geochemical elements are highly positively correlated with each other and negatively correlated with %LOI (Table 3). The exception to this pattern is Ca, which is only weakly positively correlated with the other elements (but still negatively correlated with LOI). Principal component analysis yielded 2 components responsible for 91% of the observed variance in the dataset (Table 4). Most of the geochemical elements align with PC1, responsible for 80.6% of the variance (Table 3, Fig. 5). As suggested by their correlation coefficients, most of the geochemical elements are positively correlated with PC1, while LOI is inversely correlated. Accordingly, the downcore scores for PC1 look broadly similar to elemental counts from the Itrax (Fig. 6). PC2 (10.7% of variance) shows weak correlations with most elements and LOI, but is highly positively correlated with the element Ca. We recognize that PC1 is an extension of the elemental data and we utilize the principal component analysis to highlight the similar behavior of these elements over the length of our record, and as justification for interpreting each as a record of bedrock erosion (and therefore glacial activity). In the ensuing discussion, we will consider Ti elemental abundances as a proxy for glacially derived sediment input to Gjøavatnet; however, the use of PC1 or of a different element (apart from Ca, see below) would not change any of our interpretations or conclusions.

#### 4.3. Stratigraphy and interpretation of stratigraphic units

The composite Gjøavatnet sedimentary sequence was separated into 4 major units: A, B, C, and D, and Unit C was further divided into 3 distinct subunits (Fig. 7). This determination was made based on major density transitions apparent in x-radiograph data and corresponding visual transitions between gray, silty sediment and brown, organic rich sediment (Fig. 3). Proxy data (Itrax elemental data, diatom analyses, and LOI and DBD values) were then used to inform/confirm these definitions (Table 5) (see below).

##### 4.3.1. Unit A: base of core (206.5 cm) – 11.1 cal kyr BP (162.5 cm) – Glacial till

The basal sedimentary unit, Unit A, consists of dark to light gray diamict (206.5 cm – ~170 cm), which transitions to dense silty sand (170–162.5 cm). The diamict in the lower portion of this unit is massive and poorly sorted, with individual clasts up to 5 cm in diameter. The x-radiograph of the upper section shows some faint evidence for horizontal bedding structures, but lacks the distinct laminations of later units. The unit broadly is characterized by low LOI values, ranging from 1.8% at ~11.6 cal kyr BP to ~8% at 11.2 cal kyr BP with a mean value of 3.9%. The highest dry bulk

**Table 3**

Correlation coefficients for variables used in PCA analysis.

Correlation Coefficients	Ti	Al	Si	K	Ca	Mn	Fe	Rb	Sr	LOI
Ti	1.00									
Al	0.81	1.00								
Si	0.87	0.75	1.00							
K	0.97	0.81	0.95	1.00						
Ca	0.78	0.61	0.50	0.66	1.00					
Mn	0.83	0.77	0.85	0.88	0.39	1.00				
Fe	0.84	0.72	0.90	0.90	0.34	0.94	1.00			
Rb	0.95	0.71	0.88	0.95	0.69	0.77	0.83	1.00		
Sr	0.91	0.69	0.82	0.90	0.80	0.65	0.68	0.94	1.00	
LOI	-0.91	-0.67	-0.69	-0.82	-0.85	-0.63	-0.64	-0.86	-0.85	1.00

**Table 4**

Results from PCA analysis with 8 principal components.

Principal Component #	Eigenvalue of Cov (x)	% Variance Captured this PC	Cumulative Variance Captured
1	8.08	80.6	80.6
2	1.08	10.72	91.32
3	0.39	3.87	95.19
4	0.21	2.09	97.28
5	0.11	1.05	98.33
6	0.08	0.84	99.17
7	0.05	0.48	99.64
8	0.02	0.19	99.83

density values of the entire record are found in Unit A, with a mean value of 0.71 g/cm<sup>3</sup>. Values decrease steadily from a maximum of 1.15 g/cm<sup>3</sup> at a depth of 167 cm (lowest sample) to 0.41 g/cm<sup>3</sup> at the top of the unit (Table 5, Fig. 7). Unit A has the 2nd highest average Ti counts of the entire record (1622 cps), with relatively little variation about the mean. Ca counts during the majority of this interval are the highest of any unit by nearly two orders of magnitude. They reach a maximum value of 50,014 cps and are above 30,000 cps for most of the unit (mean of 24,466 cps) (Table 5) before declining to ~1500 cps before the end of Unit A.  $\delta^{13}\text{C}$  values range from -22.2‰ to -23.7‰, with an average of -23.1‰ ( $n = 5$ ). Diatom species were analyzed in 3 samples from Unit A (dashed lines in Fig. 7). Assemblages were dominated by *Pinnularia lenticular* and *Stauroneis anceps* family (cf. *gracilis*, *vandevijveri*), which are characteristic of a silty, shallow freshwater environment (Perren et al., 2012; Wojtal et al., 2014) (Fig. 8).

One of the most interesting aspects of Unit A is the high Ca abundance during in this interval. High Ca counts are also observed in the other piston core collected from Gjøavatnet (GJP-02-14), confirming that it is a persistent feature of the sediments across the lake basin. One possible interpretation of the calcium signal is that it represents a period when the lake basin was subject to marine influence. Diatom analysis, however, has revealed that all species present at the time were freshwater-dwelling, ruling out the possibility of substantial marine influence (Fig. 8). We note here that despite the abundant driftwood on the narrow strip of land separating Gjøavatnet from the ocean today, we see no evidence in our proxy data to suggest sustained or meaningful marine influence on the lacustrine sediment record.

We interpret the high Ca abundance as a signal of bedrock erosion from the marble units within the Gjøavatnet catchment. Although the majority of the underlying bedrock consists of banded gneiss of the Smeerenburgfjorden Complex (Hjelle and Ohta, 1974; Ohta et al., 2007), there are two small outcrops of marble that would have resulted in glacially derived sediment with elevated Ca content in the northwest part of the catchment (blue outlines in Fig. 1). The exposed marble units are not being eroded by the Annabreen glacier today, but would have been subject to glacial erosion if the glacier advanced across the outcrops. We suggest that the large decrease in XRF-inferred Ca deposition to the lake c. 11.5 cal kyr BP represents the retreat of Annabreen up-valley from the marble outcrops. If this interpretation is correct, the abrupt decline in sedimentary Ca abundance ~11.4 cal kyr BP represents a threshold response as the glaciers retreated beyond the marble outcrops, and as such, we do not consider the large change in Ca abundance in our assignment of stratigraphic units.

The carbon isotopic signature of this section is also intriguing, suggesting at face value a variable but perhaps predominantly marine source (values ranging from -22.2 to -23.7‰) (Meyers, 1997). Again, however, diatom analysis has ruled out this possibility. An alternative explanation may be found in the weathering of silicate rocks and limited recycling of carbon within the catchment immediately following deglaciation (Hammarlund, 1993). Glacial activity would have resulted in a large amount of freshly weathered siliciclastic material on the landscape following deglaciation. The weathering of this material could have resulted in bicarbonate delivery to the lake water, leading to  $^{13}\text{C}$  enrichment (i.e. more positive  $\delta^{13}\text{C}$  values) of dissolved inorganic carbon and, therefore, of autochthonous organic material in the lake (Hammarlund, 1993).

We interpret Unit A to represent a period when Annabreen was terminating at or near the coring site during deglaciation of the catchment. Due to the extrapolated nature of our age model, we cannot place a definitive date on the onset of sedimentation in Gjøavatnet. The highest DBD and lowest LOI percentages are recorded during this interval, along with the presence of large individual clasts in the sediment, all of which suggest substantial glacial presence proximal to the coring site. The lowermost ~30 cm

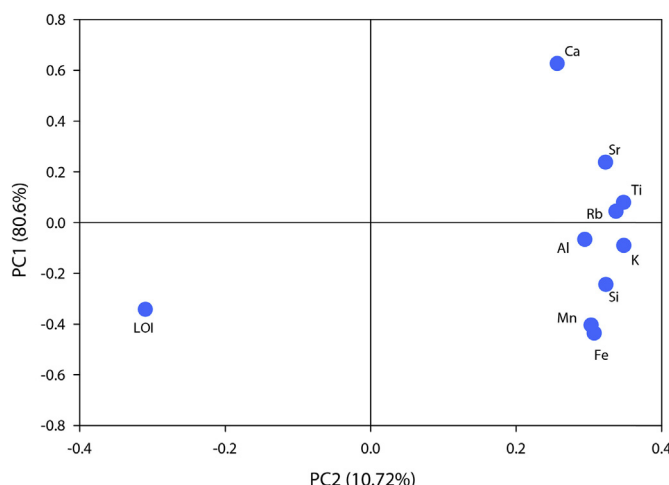
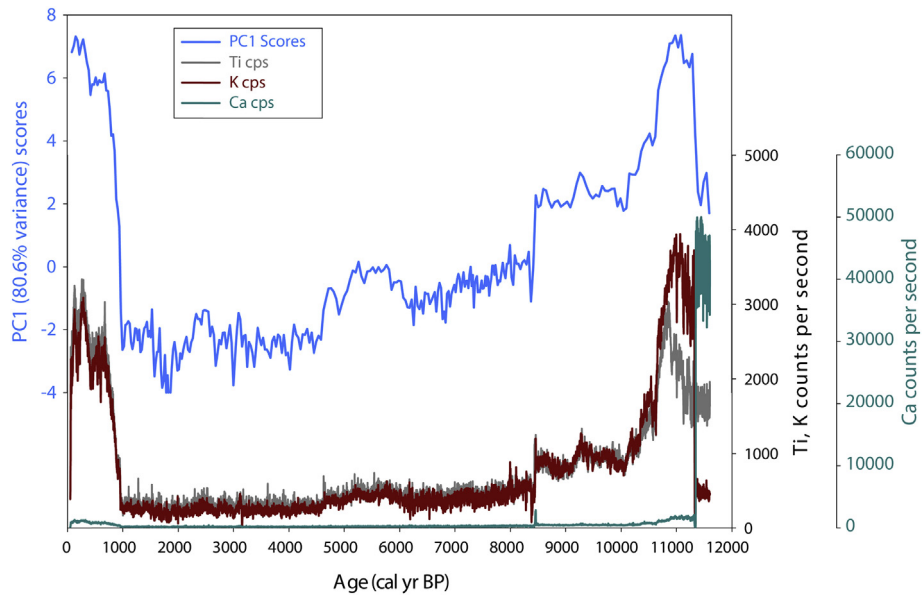
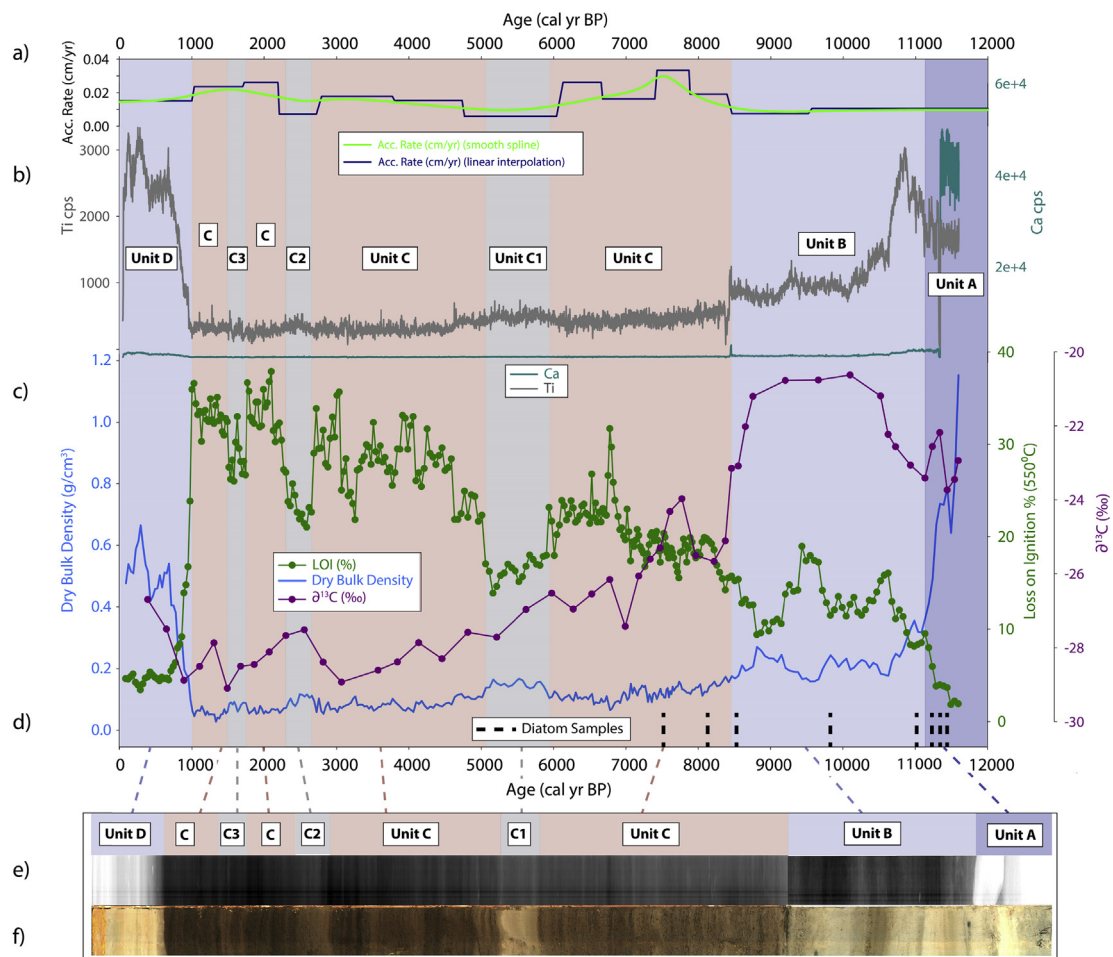


Fig. 5. Ordination diagram showing 1st (80.6% of variance) and 2nd (10.72% of variance) principal components of PCA.



**Fig. 6.** Downcore scores of 1st principal component from PCA analysis (blue line) plotted on age scale with Itrax elemental data for Ti (gray), K (dark red) and Ca (cyan) for core GJP-01-14. Note different scale for Ca data relative to Ti and K. (For interpretation of the references to colour in this figure legend, the reader is referred to the web version of this article.)

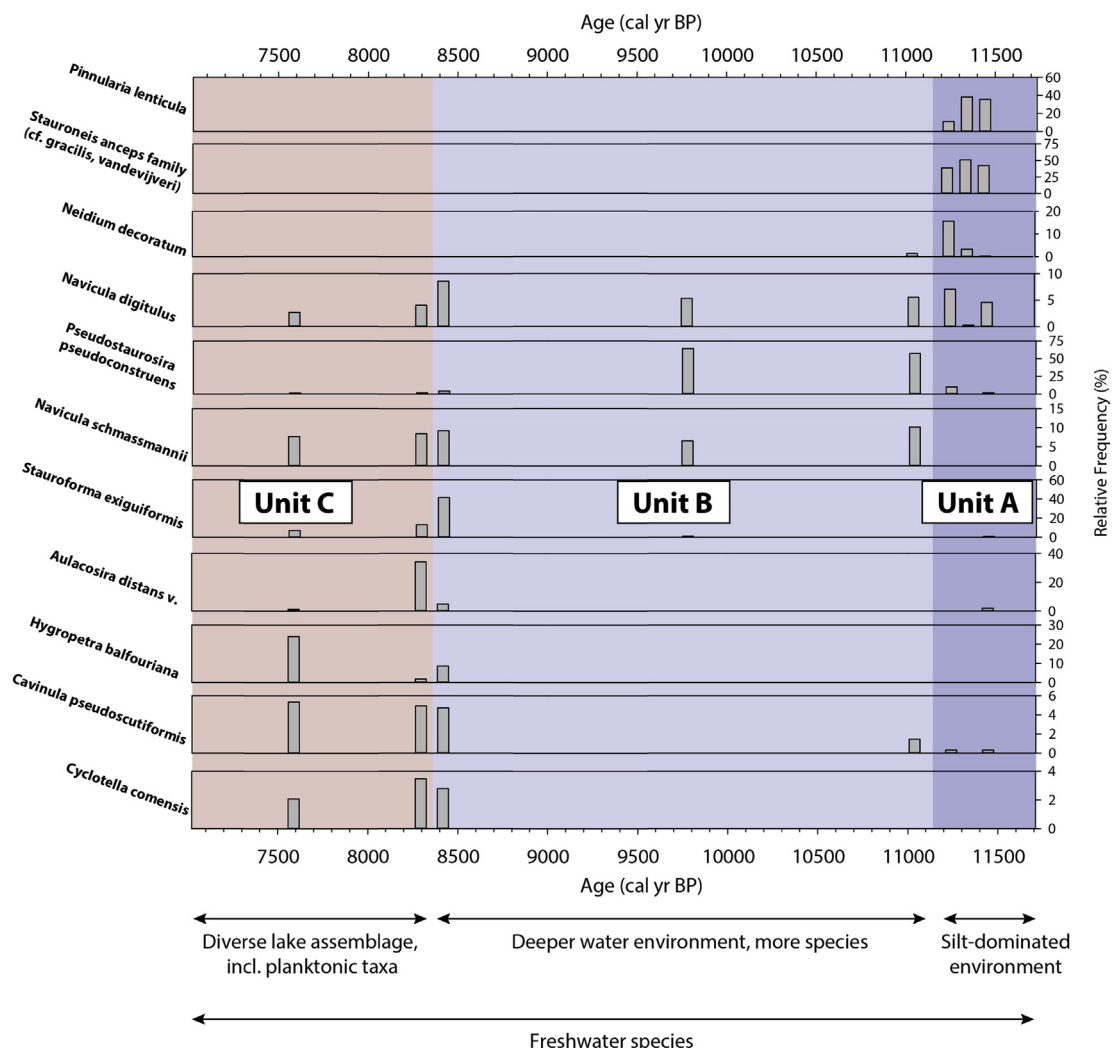


**Fig. 7.** Downcore proxy results for GJP-01-14. Shaded background colors denote different sedimentary units (Units A-D). a) Sediment accumulation rates based on smooth spline interpolation (light green) and linear interpolation (dark blue) between radiocarbon dates; b) Itrax elemental data showing Ti (gray) and Ca (cyan) (note different scales); c) Loss-on-ignition (dark green), bulk  $\delta^{13}\text{C}$  (purple) and dry bulk density values (dark blue); d) location of diatom taxonomy samples (black dashed lines); e) X-ray image and f) normal image of GJP-01-14 core. Light/white shades in e) denote denser material.

**Table 5**

Relevant proxy data for sedimentary units identified in Gjøavatnet record.

Unit	Depth Range (cm)	Approx. Age Range (cal kyr BP)	Avg. Ca cps	Avg. Ti cps	Avg. DBD (g/cm <sup>3</sup> )	Avg. LOI	Avg. Acc. Rate (cm/kyr)	Avg. $\delta^{13}\text{C}$ (‰)
Unit A	209.5–162.5	Base – 11.1	24,466 <sup>a</sup>	1623 <sup>a</sup>	0.71 <sup>a</sup> n = 9	3.9 <sup>a</sup> n = 9	9.8	–23.0 n = 5
Unit B	162.5–136.5	11.1–8.4	655	1174	0.22 n = 56	13.0 n = 56	9.7	–22.2 n = 13
Unit C	136.5–16.5	8.4–1.0	231	372	0.09 n = 198	25.5 n = 198	18.4	–27.1 n = 24
Unit C1	89.5–81	5.9–5.0	253	489	0.15 n = 18	16.5 n = 18	10.1	–27.3 n = 2
Unit C2	48.5–42	2.7–2.2	199	341	0.10 n = 14	24.0 n = 14	15.7	–27.6 n = 2
Unit C3	32–27	1.7–1.5	174	279	0.08 n = 11	28.2 n = 11	21.6	–28.5 n = 1
Unit D	16.5–0	1.0 – present	785	2157	0.43 n = 29	6.9 n = 29	15.7	–27.7 n = 3

<sup>a</sup> Data collected down to a depth of ~167 cm.**Fig. 8.** Percent abundance of diatom taxa throughout the early evolutionary history of Gjøavatnet. Note sedimentary unit delineations (labels and background shaded colors) that correspond with Fig. 7.

of GJP-01-14 is comprised of glacial till/diamict, which was likely deposited when the glacier was directly adjacent to (or overriding) the coring site. We speculate that the remainder of Unit A (~167–162.5 cm), when DBD values were still relatively high, represents a period when Annabreen was likely terminating within the

lake.

The boundary between Unit A and Unit B at ~11.1 cal kyr BP is primarily defined by DBD values, a shift in diatom species, and a major density change seen in the x-radiograph data (Fig. 3). The diatom samples below the transition represent a silt-dominated

environment (e.g. Perren et al., 2012), as would be expected if Annabreen was terminating within the lake or was contributing a significant amount of meltwater to the lake system, whereas the samples above (in Unit B) are more diverse and point to a reduction of suspended silt in the water column. Together, these proxies suggest that while Annabreen was still active during the deposition of Unit B (see below), it was reduced in size and/or influence compared to Unit A.

#### 4.3.2. Unit B: 11.1 cal kyr BP (162.5 cm) – 8.4 cal kyr BP (136.5 cm) – Deglaciation of Gjøavatnet catchment

Unit B consists of a mixture of gray, laminated, clayey silt interbedded with relatively organic rich brown material. It is characterized by generally low but variable LOI values ranging from 8.1 to 19% (mean of 13.0%) (Fig. 7). DBD values (0.14–0.36 g/cm<sup>3</sup>; mean of 0.22 g/cm<sup>3</sup>) are relatively high during this unit, though much lower than in preceding Unit A. Ti counts are higher in the lower portion of this unit than Unit A, increasing to a maximum of 3034 counts at ~10.8 cal kyr BP before decreasing to ~800–1000 cps for the majority of the Unit B. Ca counts in Unit B are significantly lower than in Unit A, decreasing from ~1500 counts at the base of Unit B to ~300 cps (average value of 655 cps).  $\delta^{13}\text{C}$  values are the most enriched in this section of the core, rising from ~−23.5‰ at 162.5 cm to a value of ~−21‰ (average of −22.2‰,  $n = 13$ ).

Three samples from Unit B were analyzed for diatom taxonomy. Assemblages in the lowermost two samples are dominated by *Navicula (Genkalia) digitulus* and *Pseudostaurosira pseudoconstruens* and also contain the first appearance of *Navicula schmassmannii* in the sediment record (Fig. 8). These species are characteristic of a deeper lake with less suspended silt than the species from Unit A (Perren et al., 2012). The third sample, taken at a depth of 137 cm (approx. 8.6 cal kyr BP), is characterized by a more diverse assemblage including *Stauroforma exiguiformis*, *Hyropetra balfouri-ana*, and *Aulacoseira distans*.

We interpret Unit B to represent an interval when Annabreen was still present within the catchment, but likely not terminating within the lake. The two oldest diatom samples from this interval (~11 and 9.7 cal kyr BP) (Figs. 7 and 8) are characteristic of a deeper lake with less suspended silt load than during the deposition of Unit A. Elemental abundance data (Figs. 6 and 7) suggest a broad decrease in the influence of Annabreen on the sediment record across this interval, although reductions in elemental counts occur in a stepwise fashion (cf., Ti counts). The %LOI trend across Unit B is also non-linear and is quite variable at multi-centennial timescales (Fig. 7), suggesting the glacier may have been fluctuating dynamically during this time and/or that sedimentation was influenced by glaciofluvial dynamics in the glacier forefield as ice retreated. The third diatom sample from this section (just prior to 8.4 cal kyr BP) (Fig. 8) reveals a more diverse assemblage than the two older samples from Unit B, including planktonic taxa. Again, this assemblage suggests Annabreen's influence on sedimentation in the lake waned throughout this period.

Bulk organic carbon isotope values in Unit B are the most positive of the record, with a mean of −22.2‰. Such a value is generally associated with marine algae (Meyers, 1997), however, only freshwater diatom species are found in the Gjøavatnet sediment record, precluding a marine source for the relatively  $\delta^{13}\text{C}$ -enriched carbon isotope values. As discussed above, a possible explanation is the weathering of glacial flour derived from silicate rocks during this time that could have increased the  $\delta^{13}\text{C}$  value of DIC (dissolved inorganic carbon) in Gjøavatnet (Hammarlund, 1993).

The boundary between Unit B and Unit C at ~8.4 cal kyr BP is marked by an increase in LOI, an abrupt decrease in Ti abundance, and a concomitant shift in  $\delta^{13}\text{C}$  values (Figs. 6–8). It is apparent that

the nature of sedimentation in Gjøavatnet changed dramatically at this point. The most likely explanation is the disappearance, or the dramatic reduction in size, of the Annabreen glacier at ~8.4 cal kyr BP.

#### 4.3.3. Unit C: 8.4 cal kyr BP (136.5 cm) – 1.0 cal kyr BP (16.5 cm)

**4.3.3.1. Non-glacial sedimentation in Gjøavatnet.** Unit C comprises the majority of the sediment record from Gjøavatnet (120 cm of ~206 total) and is composed of laminated brown organic rich sediment with interbedded gray minerogenic layers. The highest LOI values of the entire core are recorded in Unit C, and generally follow a linear increasing trend from ~18% to 35% (average of 25.5%) (Fig. 7). This linear trend is interrupted by at least three distinct multicentennial-scale intervals characterized by abrupt shifts to relatively lower LOI values, higher Ti and DBD values, and decreases in sedimentation rate. These subunits are defined as C1 (81–89.5 cm, ~5.0–5.9 cal kyr BP); C2 (42–48.5 cm, 2.2–2.7 cal kyr BP); and C3 (27–32 cm, 1.5–1.7 cal kyr BP). Proxy data for these three subunits are compared to average values from the remainder of Unit C, and presented in Table 5, to examine the differences between these subunits and Unit C in general. DBD values for Unit C generally follow the inverse trend of LOI, beginning at ~0.15 g/cm<sup>3</sup> and declining to a minimum of 0.03 g/cm<sup>3</sup> near the top of the section. Ti counts are generally low throughout this portion of the record, ranging from 88 to 661 cps with an average value of 372 cps. Ca counts are extremely low in Unit C, averaging 231 counts (max of 305 cps, min of 69 cps), with little variation. During the deposition of this sedimentary unit we interpret Ti abundances to reflect catchment dynamics unrelated to glacier activity (e.g., such as changes in runoff), or dilution by increased organic matter deposition.

Carbon isotope values in Unit C increased from ~−25.5‰ to −24‰ at 7.6 cal kyr BP and then steadily decreased to −28.5‰ (average value of −27.1‰). Two samples analyzed for diatoms from the base of this unit, at ~8.1 (135.5 cm depth) and 7.6 cal kyr BP (121.5 cm depth), show similar assemblages to the uppermost sample from Unit B (Fig. 8), revealing a diverse community including planktonic diatoms living in the upper water column.

We interpret Unit C to represent a phase during the Holocene when the Annabreen glacier either completely melted away or was too small to influence sedimentation in the lake. Ti counts and DBD are at their lowest during this period (Table 5, Fig. 7). Bulk  $\delta^{13}\text{C}$  values during this period average −27.1‰, likely reflecting a lacustrine algal source (−25 to −30‰) (Meyers, 1997). LOI values increase from ~20% at ~8.0 cal kyr BP to nearly 40% near the transition to Unit D at 1.0 cal kyr BP. An increasing trend in % organic matter during the Holocene has also been observed in other Svalbard lakes (e.g. Gjerde et al., in press; van der Bilt et al., 2015) and is attributed to lake and catchment ontogeny and greater nutrient recycling. The trend may have also have been influenced by increasing preservation of organic matter, as declining summer insolation potentially shortened the ice-free season resulting in greater bottom water anoxia or hypoxia (Laskar et al., 2004).

**4.3.3.2. Interpretation of subunits C1, C2, and C3.** Unit C is punctuated by abrupt transitions between brown, organic-rich sediment and gray, more minerogenic sediments (the latter defined as sub-units C1–C3; Fig. 7). These transitions are apparent in LOI, visual stratigraphy, x-radiograph images, and DBD values. These units appear massive, with few laminations. Subunits C1–C3 could represent: (i) short-lived advances of the Annabreen glacier, (ii) slump activity (e.g. turbidites), or (iii) periods of reduced organic matter accumulation. We suggest that advances of Annabreen are not likely to have caused these changes because sediment

characteristics during subunits C1, C2, and C3 are not consistent with other intervals associated with glacial erosion in the catchment (Units A, B, D). Ti counts are much lower in the Unit C sub-units, for example (Fig. 7). Additionally, the relationship between Ti and %LOI is broadly similar across Unit C and subunits C1–C3 relative to Units A, B and D, inferred to represent a glacial signature (Fig. 9). Furthermore, the timing of Unit C1 corresponds with the interval when nearby lake Hakluytvatnet completely dried out, likely in response to dry conditions (c. 7.7–5.0 cal kyr BP), suggesting the precipitation regime was not favorable for the regrowth of Annabreen (Gjerde et al., in press; Balascio et al., in press). It is also unlikely that these subunits were the result of slump events. Radiocarbon dates from either side of both units C1 and C2 were used to quantify sedimentation rates across each interval using a linear interpolation between data points (Fig. 7), and indicate that sedimentation rates slowed during deposition of these subunits. Mass wasting events, such as slumping, would lead to an increase, not a decrease in sedimentation rate.

We therefore interpret subunits C1, C2, and C3 as intervals of reduced organic productivity, most likely driven by periods of prolonged summer lake ice cover and/or drier and colder conditions on Amsterdamøya. Sediment was likely delivered to the lake during a short period of reduced ice cover during the summer, which may have been potentially limited to a moat around the lake edge.

#### 4.3.4. Unit D: 1.0 cal kyr BP (16.5 cm) – present - Re-advance of Annabreen

The uppermost stratigraphic unit, Unit D, is characterized by an abrupt shift to gray, minerogenic sediment with faint laminations and a small number of sand sized grains (visually identified from the split core). Unit D is characterized by low LOI values (mean of 6.9%) and high DBD (mean of 0.43 g/cm<sup>3</sup>) (Table 5). The dense nature of Unit D is also evident from the X-radiograph (Fig. 7). Ca counts increase in this unit relative to Unit B (average of 785 vs. 231), but remain nearly two orders of magnitude lower than Unit A

at the base of the core. Bulk  $\delta^{13}\text{C}$  values increase from  $-28.9\text{\textperthousand}$  to  $-26.7\text{\textperthousand}$  across the three samples representing this section. Ti counts in Unit D are the highest of the entire record (mean of 2127 cps).

We interpret Unit D to represent the reemergence of the Annabreen glacier, though this could also represent the transition from residual cold-based ice to a polythermal glacier. The youngest radiocarbon date from the Gjøavatnet record was taken just below this transition, allowing confident age assignment to the boundary. Although there are only three  $\delta^{13}\text{C}$  samples from this interval, we note that they increase from  $-28.9\text{\textperthousand}$  to  $-26.7\text{\textperthousand}$ , a change similar in magnitude to the pattern seen at the beginning of Unit B, which is likely related to increased glacial erosion and delivery of relatively  $^{13}\text{C}$ -enriched material to the lake (Hammarlund, 1993).

#### 4.3.5. Summary

The sedimentary units described here represent the broad phases of environmental change within the Gjøavatnet catchment. Unit A represents the period when Annabreen was likely larger than today and much of the catchment covered by ice. We infer that the glacier was terminating within the lake during this time. The transition to Unit B at  $\sim 11.1$  cal kyr BP likely marks the time when Annabreen retreated from the lake basin. We propose that the glacier was present in the Gjøavatnet catchment until  $\sim 8.4$  cal kyr BP. From  $\sim 8.4$ – $1.0$  cal kyr BP the glacier was absent or had become dramatically diminished in size, and variations in sediment properties were likely controlled primarily by changes in summer temperature and/or the duration of the summer ice free season. At  $\sim 1$  cal kyr BP the local ELA lowered enough to allow Annabreen to reform, and the glacier has been terminating in the lake since that time.

### 5. Regional paleoclimate context of Gjøavatnet record

#### 5.1. Early Holocene: deglaciation of Amsterdamøya

During the Last Glacial Maximum, ice extended all the way to the shelf edge in NW Svalbard,  $\sim 8$  km offshore (Ingólfsson and Landvik, 2013). During this time it is likely that the majority of the Gjøavatnet catchment was covered by ice, although the  $>300$  m high plateaus on the island have been ice free for at least 80 cal kyr BP (Landvik et al., 2003). Ice began to retreat from the shelf edge sometime prior to 14 cal kyr BP, reaching the coast of NW Svalbard by  $\sim 13.8$  cal kyr BP (Ingólfsson and Landvik, 2013). The deglaciation of the nearby Hakluytvatnet catchment at  $\sim 12.8$  cal kyr BP suggests some small cirques on the island were largely ice-free by this time (Gjerde et al., in press). However, Annabreen was still terminating near the coring site in Gjøavatnet for another  $\sim 1.7$  kyr until it retreated out of the lake basin at  $\sim 11.1$  cal kyr BP and then disappeared, or at least greatly diminished in size, at 8.4 cal kyr BP.

Proglacial lake records from the nearby Mithrahalvøya peninsula also point to a complex deglacial history in western Svalbard, with the catchment of Lake Kløsa deglaciating  $\sim 9.2$  cal kyr BP (Røthe et al., 2015), while glacial ice persisted in the catchment of Lake Hajeren until  $\sim 7.4$ – $6.7$  cal kyr BP (van der Bilt et al., 2015) (Fig. 10). Further south in the Linné valley, the Linnébreen glacier and another small cirque glacier in the same area are believed to have melted away during the early Holocene (Svendsen and Mangerud, 1997; Snyder et al., 2000; Reusche et al., 2014). Lacustrine alkenone-based temperature reconstructions from Amsterdamøya and the Mithrahalvøya peninsula also point to warm conditions before  $\sim 8$  kyr BP (van der Bilt et al., 2016).

The proposed final deglaciation of the Gjøavatnet catchment ( $\sim 8.4$  cal kyr BP) occurred during a prolonged period of warm surface water conditions in Fram Strait (Müller et al., 2012; Werner

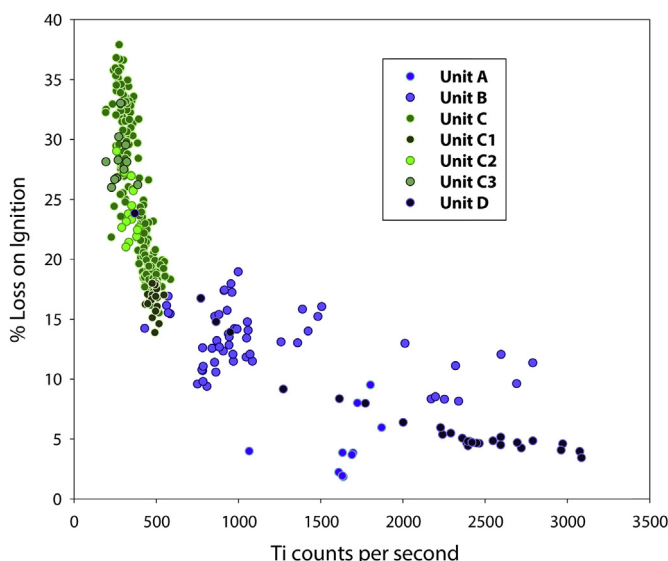


**Fig. 9.** Relationship between % Loss-on-ignition (LOI) and Ti counts from Itrax. Data from sedimentary units when Annabreen glacier is interpreted to be present are shown in blue shades (Unit A, B, D); data from units when Annabreen interpreted to be absent are shown in green shades (Unit C, C1, C2, C3). (For interpretation of the references to colour in this figure legend, the reader is referred to the web version of this article.)

et al., 2013, 2015; Rasmussen et al., 2014). Aagaard-Sorensen et al. (2014) found the warmest Mg/Ca based temperatures in their record from core MSM5/5-712-2 from ~10.5–7.9 kyr BP. IP<sub>25</sub> concentrations (a biomarker indicative of diatoms associated with sea ice) (Belt et al., 2007) from the same core also suggest the region experienced “significantly reduced ice cover” between 8.2 and 7.8 cal kyr BP (Müller et al., 2012). IP<sub>25</sub> concentrations in the nearby MSM5/5-723-2 core also suggested warm temperatures and low concentrations of sea ice during the period ~11–7 kyr BP (Werner et al., 2015). Foram-based temperatures also suggest increased advection of warm Atlantic water into this part of Fram Strait during this time (Werner et al., 2013). While we acknowledge the possibility that Annabreen was dramatically reduced in size during the mid-Holocene (or became a cold-based glacier with little

erosive power), we point to warming trends seen in marine records, along with evidence that many other glaciers in Svalbard melted away during this time (Fig. 10), as strong evidence for our interpretation that the glacier melted away.

Warmer conditions following deglaciation generally define the early Holocene climate of this region, although periodic cooling events have been identified in the North Atlantic and attributed to freshwater forcing (Sejrup et al., 2016). The “8.2” event (Alley et al., 1997) is the most prominent of these, although we do not see it expressed in the Gjøavatnet record, a finding that echoes another similar study from Svalbard (van der Bilt et al., 2015). It may be that dry conditions during this time (Rohling and Pälike, 2005), coupled with its brief duration (Thomas et al., 2007), prevented Annabreen from re-growing sufficiently to impact the sediment in Gjøavatnet.

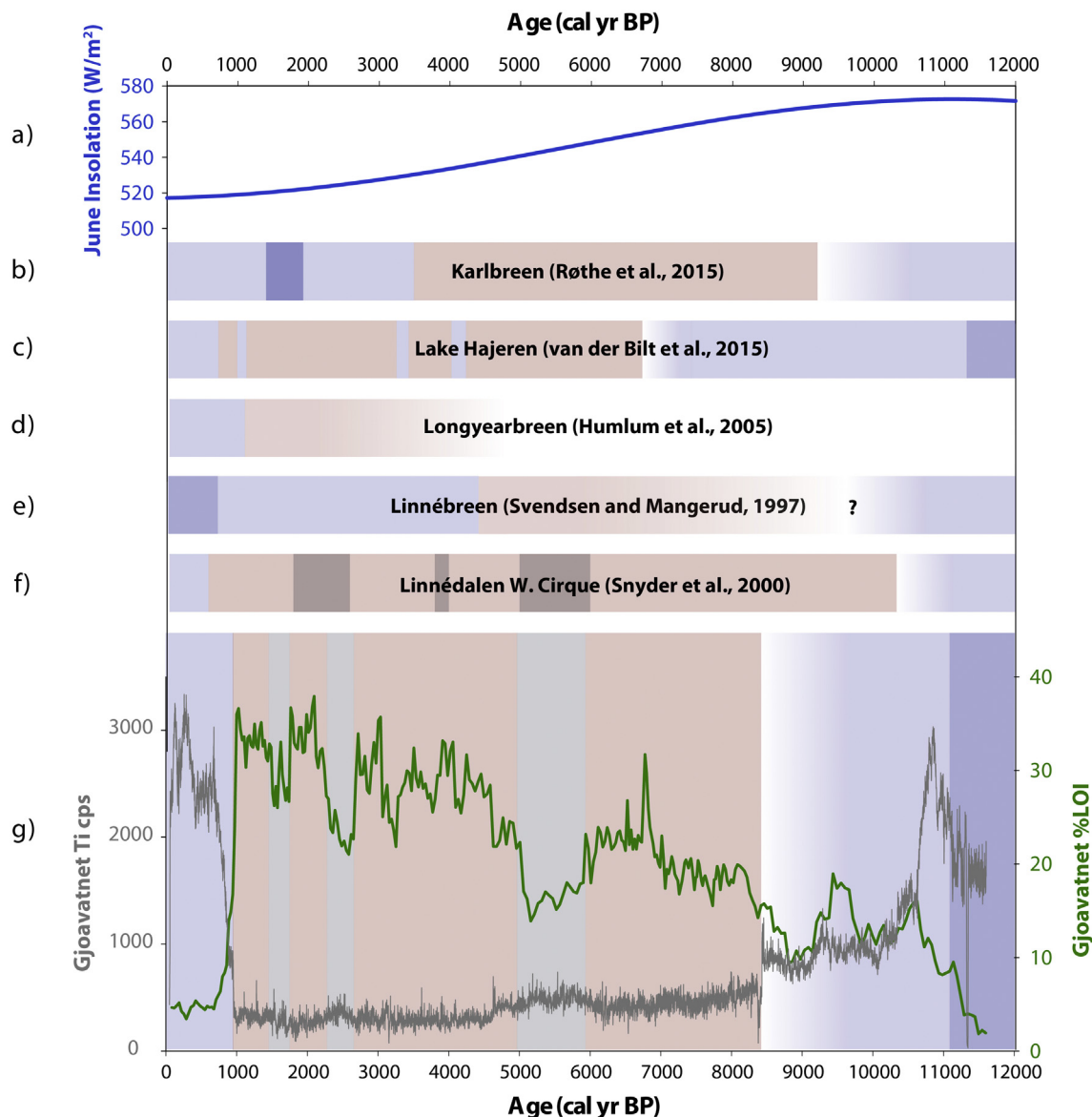


**Fig. 10.** Holocene glacial activity reconstructions from Svalbard: a) June insolation values at 79°N over the Holocene (Laskar et al., 2004); schematic depiction of glacier activity in Svalbard based on published reconstructions: b) and c) proglacial lake reconstructions from Mitråhalvøya peninsula (Røthe et al., 2015; van der Bilt et al., 2015); d) proglacial paleosol and vegetation study (Humlum et al., 2005); e) & f) proglacial lake records from Linnévatnet (Svendsen and Mangerud, 1997; Snyder et al., 2000); g) %LOI and titanium counts from Gjøavatnet (this study). Blue boxes represent periods of glacial activity (dark blue = enhanced glacial activity), red boxes suggest no glacier was present in the catchment or glacial activity was greatly reduced; gray boxes indicate periods of reduced organic matter accumulation (Gjøavatnet) or increased laminations (Snyder et al., 2000) that are not interpreted as glacial activity. (For interpretation of the references to colour in this figure legend, the reader is referred to the web version of this article.)

## 5.2. Middle Holocene – sea ice and freshwater influences on Amsterdøya climate

During the middle Holocene period on Amsterdøya (~8–1 cal kyr BP), we propose that Annabreen was absent from the catchment. This period is punctuated by periodic decreases in organic matter accumulation in the lake (subunits C1–C3). We hypothesize that the most likely mechanism for these intervals is an abrupt change in temperature and/or precipitation (we note these two parameters are positively correlated today (Førland et al., 2011)), which at this maritime location would most likely be driven by offshore oceanographic conditions. Periodic increases in freshwater input and the presence of a surface freshwater layer (and likely accompanying sea ice) could dramatically lower both temperature and precipitation near Gjøavatnet, leading to the reduction in organic matter accumulation seen during the subunits. Interestingly, Unit C1 occurs during a period of increased deposition of discrete laminae in Linnévatnet (Snyder et al., 2000) (grey shaded area in Fig. 10). The deposition of Unit C1 also occurs during a hiatus in sedimentation in nearby Hakluytuvatnet (Gjerde et al., in press), suggesting dry conditions on Amsterdøya during this time. Numerous authors have suggested the presence of a freshwater cap or lens near Svalbard during the Middle Holocene (Rasmussen et al., 2013; Werner et al., 2013, 2015), although the exact timing and magnitude of this oceanographic feature remains somewhat ambiguous. With respect to the most prominent of the subunits, C1, there does appear to be complimentary evidence for oceanographic changes during the period ~6–5 cal kyr BP.

Multiple marine records from near Svalbard and in the Fram Strait have found evidence for an increased flux of cold water from the Arctic around 6 cal kyr BP. Ślubowska et al. (2005, 2007) found increases in the concentrations of the benthic foraminifera *E. excavatum*, characteristic of Arctic ocean water, at ~6.8 and 6 cal kyr BP north of Svalbard. Ebbesen et al. (2007) cite a shift in  $\delta^{18}\text{O}$  values of foraminiferal tests at 6 cal kyr BP as evidence for a change in the relative contributions of water masses off western Svalbard. Numerous studies have also shown that the thermophilous mollusk, *Mytilis edulis*, likely died out in northern Svalbard around 6–5 cal kyr BP (Blake, 2006; Salvigsen, 2002). Evidence from a proglacial fjord record in Nordauslandet points to the rapid deposition of a glacial diamict between 5.8 and 5.7 cal kyr BP (Kubischa et al., 2011). These reconstructions suggest broadly cooler conditions prevailed during the hiatus in Hakluytuvatnet and the deposition of Unit C1 in Gjøavatnet.

Interestingly, multiple proxy reconstructions from the Fram Strait, just west of Amsterdøya (Fig. 1), suggest there was warm and saline water in the subsurface ocean (~depth of 100 m) during this time (Werner et al., 2013; Aagaard-Sørensen et al., 2014). Two proxies for sub-surface seawater temperature from core MSM5/5-712-2 depict warm temperatures from 6.1 to 5.2 ka (Werner et al., 2013; Aagaard-Sørensen et al., 2014) (Fig. 11). The warm, saline water is presumed to be Atlantic-sourced water carried by the WSC. Werner et al. (2013) attribute the subsurface temperature increase to insulation by cold, fresh water at the surface that limited heat loss to the atmosphere. These hydrographic conditions suggest an increased amount of cold, fresh meltwater (and also associated sea ice) near Amsterdøya during this time. The subsurface warmth is not a feature of all temperature records from the Fram Strait, however. The foram-based subsurface temperature reconstruction from nearby core MSM5/5-723-2 (Werner et al., 2015) instead suggests that a broad cooling trend began around 6 kyr BP. 6 kyr BP also marks the beginning of a decline in both the concentration of subpolar planktic forams and reconstructed subsurface (75 m depth) temperatures in the Kongsfjorden Trough (Rasmussen et al., 2014).

Local sea ice reconstructions also do not support the notion of dramatic increases in sea ice in eastern Fram Strait from ~6 to 5 kyr BP. IP<sub>25</sub> concentrations from cores MSM5/5-723-2 and MSM5/5-712-2 are broadly stable during this time, as are IRD concentrations (Fig. 11) (Müller et al., 2012; Werner et al., 2013, 2015). Interestingly, however, relatively high IP<sub>25</sub> concentrations are found on the East Greenland Shelf from ~6.5–5.6 kyr BP, the only extended period of high IP<sub>25</sub> accumulation until ~1.0 cal kyr BP (Müller et al., 2012). Funder et al. (2011) also inferred increased export of multiyear sea ice out of the Fram Strait after 6 kyr BP, based on driftwood deposits on the coast of East Greenland.

Further afield, numerous marine records from the north of Iceland also suggest oceanographic changes were occurring ~6–5 cal kyr BP. Castañeda et al. (2004) and Knudsen et al. (2004) both cite cooling trends beginning at 6.2 and 6.0 cal kyr BP respectively, while the alkenone based SST record of Mooszen et al. (2015) shows a similar cooling trend beginning at this time (Fig. 11). There is also evidence for an increase in sea ice concentrations north of Iceland beginning at 6.2 cal kyr BP (Cabedo-Sanz et al., 2016). Risebrobrakken et al. (2011) cite 6 cal kyr BP as the end of the Holocene Thermal Maximum in the North Atlantic, based on 6 cores from the Nordic and Barents Seas. Further south in the Atlantic basin Hoogakker et al. (2011) suggest 6.5 cal kyr BP was the start of a major reorganization of water masses associated with deep ocean circulation. Our C1 subunit also aligns with the largest so-called Bond Event of the Holocene (Bond Event #4) identified in a marine record in the North Atlantic (Bond, 2001) (Fig. 11).

Although there is not a clear relationship between these offshore records and the timing of subunits C2 (c. 2.7–2.2 kyr BP) and C3 (c. 1.7–1.5 kyr BP), the IP<sub>25</sub> concentration record of Müller et al., 2012, shows the highest accumulation rates of IP<sub>25</sub> in the entire record during subunit C3 (Fig. 11). A minor dip in LOI concentrations in Gjøavatnet at ~3.2 cal kyr BP, which is one of the most pronounced in the Hakluytuvatnet record (Gjerde et al., in press), does appear contemporaneous with a spike in IRD in the record of Werner et al. (2013) as well. Similar to the 6–5 cal kyr BP interval, many of the marine records from the Fram Strait suggest a warming of subsurface waters and an increase in meridional overturning circulation after 3 ka (e.g. Sarnthein et al., 2003; Rasmussen et al., 2013; Berben et al., 2014; Werner et al., 2015) while simultaneously suggesting increased sea ice cover at the surface (Müller et al., 2009, 2012; Werner et al., 2015).

In summary, it appears there is evidence for greater subsurface warming and increased Atlantic advection around 6–5 kyr BP (Werner et al., 2013, 2015; Aagaard-Sørensen et al., 2014), as well as increased sea ice concentrations in the western part of the Fram Strait (Funder et al., 2011; Müller et al., 2012), when we infer cold conditions on Amsterdøya. The agreement between the end of unit C1 in Gjøavatnet and the resumption of sedimentation in nearby Hakluytuvatnet also points to a wider forcing beyond the lake catchment itself. We propose similar oceanographic conditions may have existed during the deposition of subunits C2 and C3.

## 5.3. Late Holocene advance of Annabreen glacier

The sediment record from Gjøavatnet clearly indicates that input of mineralogenic material, formed by bedrock erosion by the Annabreen glacier, abruptly began again ~1.0 cal kyr BP, and that this input has continued up to the present day. Other terrestrial records also suggest glaciers began to regrow around Svalbard around this time (Snyder et al., 2000; Humlum et al., 2005; van der Bilt et al., 2015), although Karlbreen on Mitrahalvøya appears to have begun to re-advance earlier (~3.5 cal kyr BP) (Røthe et al., 2015). Linnebreen also began to regrow much earlier in the Holocene (~4–5 cal kyr BP), but is believed to have reached its

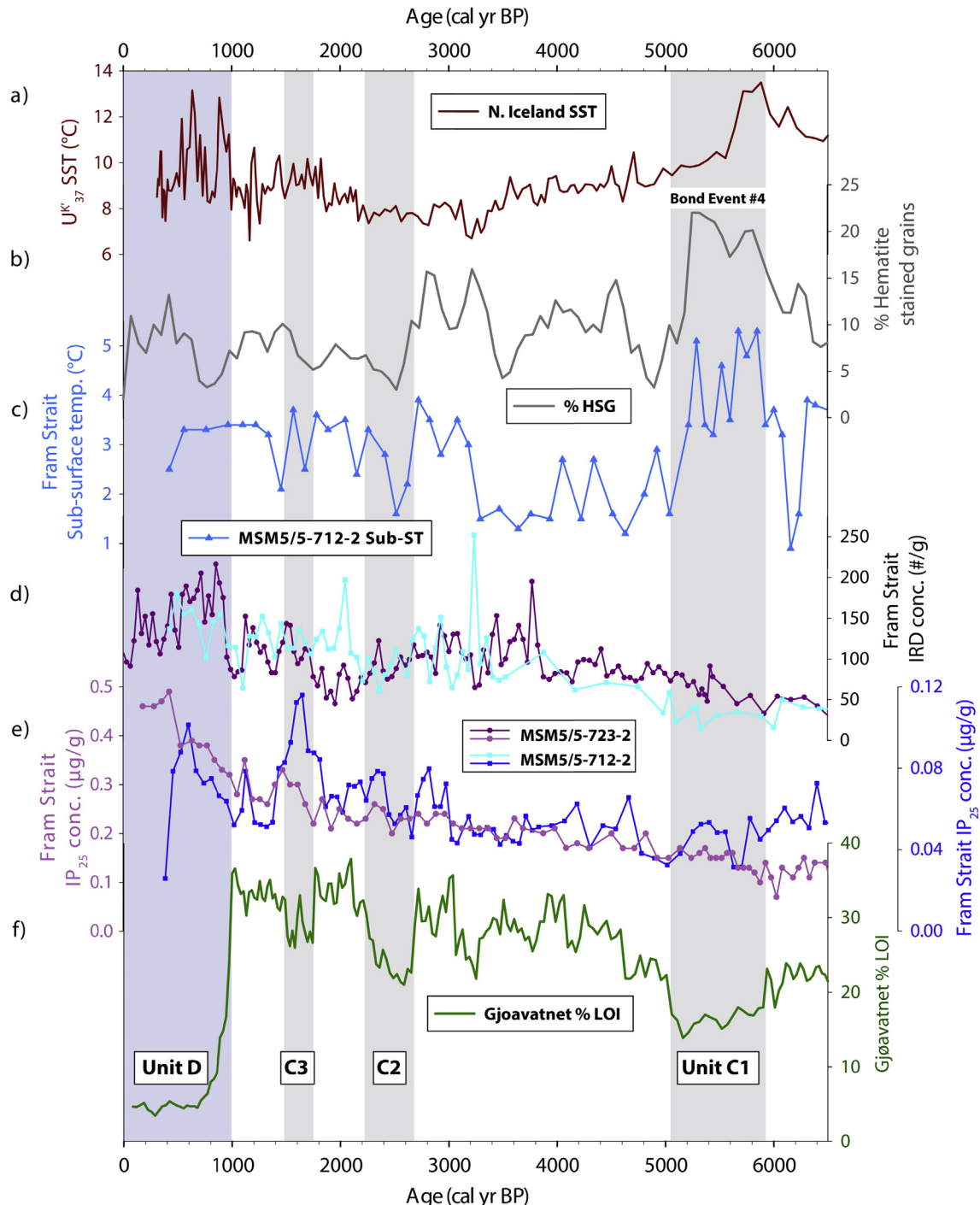


**Fig. 11.** Compilation of relevant paleoclimate data from NW Svalbard, Fram Strait, and Davis Strait: a) Alkenone based sea-surface temperatures from NW Icelandic shelf (Moosse et al., 2015); b) % hematite stained grains from core VM29-191 as a proxy for drift ice, w/Bond Event #4 labeled (Bond, 2001); c) sub-surface (~100 m depth) foram-based temperatures from core MSM5/5-712-2 (Werner et al., 2013) and MSM5/5-723-2 (purple circle data points) (Werner et al., 2015) from Fram Strait; d) IRD counts and e) IP<sub>25</sub> concentrations from core MSM5/5-712-2 (cyan/blue square data points) (Werner et al., 2013) and MSM5/5-723-2 (purple circle data points) (Werner et al., 2015) from Fram Strait; f) % loss-on-ignition data (green) from Gjøavatnet lake. Background shaded colors refer to sedimentary units from Gjøavatnet record (Fig. 7). (For interpretation of the references to colour in this figure legend, the reader is referred to the web version of this article.)

maximum Holocene extent during the 18–19th centuries (Svendsen and Mangerud, 1997). Offshore marine records also suggest broad cooling conditions ~1.0 cal kyr BP. Werner et al. (2015) posit that elevated advection of North Atlantic waters into the eastern Fram Strait region likely ended around 1.0 kyr BP. Evidence for seasonal sea ice and unstable oceanographic conditions was found south of Svalbard in the western Barents Sea after 1.1 kyr

BP (Berben et al., 2014) and Hald et al. (2004) point to a peak in IRD off western Svalbard at 0.8 cal kyr BP.

It remains unclear whether colder summer temperatures or increased wintertime precipitation led to the reemergence of Annabreen. Temperature reconstructions from Kongressvatnet (D'Andrea et al., 2012), as well as from Lake Skardtjørna (Velle et al., 2011), both on western Svalbard, suggest that summer

temperatures were relatively stable during the past 1800 years, prior to recent anthropogenic warming.

## 6. Conclusions

This paper reports a Holocene reconstruction of the Annabreen glacier from Lake Gjøavatnet on Amsterdamøya, NW Svalbard. We show that sedimentation was dominated by glacial activity in the catchment during the early and late Holocene and likely responded to regional-scale oceanographic changes in the intervening period. The early Holocene interval in Gjøavatnet is characterized by a two-phase sedimentation history, with Annabreen retreating out of the lake catchment ~11.1 kyr BP and shrinking to its minimum Holocene extent by ~8.4 kyr BP. During the period from ~8.4–1.0 cal kyr BP it seems likely there was no glacial influence on sedimentation in Gjøavatnet. The organic-rich sediments deposited during this time are interrupted by at least three intervals of lower organic matter content (c. 5.9–5.0 kyr BP, 2.6–2.2 kyr BP, and 1.7–1.5 kyr BP). We interpret the reductions in organic carbon content as periods of more extensive summer lake ice cover (due to colder summer conditions) related to changing oceanographic conditions in Fram Strait. At c. 1.0 cal kyr BP Annabreen re-advanced to the extent that it dominated sedimentation in the lake.

Maritime lakes in places like Svalbard provide the opportunity to capture both local glacier fluctuations along with offshore oceanographic conditions. Marine records are generally lower resolution than their lacustrine counterparts, and incorporate information from the entire water column, potentially complicating the detection of short-lived oceanographic events. Ocean based reconstructions over the Holocene near Svalbard suggest a complex and variable water mass and climate history, which we propose can be informed by the high-resolution lacustrine record from Gjøavatnet. While more research from both the terrestrial and marine realms would help confirm the climate patterns identified here, this study provides a unique record of both local glacial fluctuations and offshore oceanographic conditions spanning the Holocene.

## Acknowledgments

Permission to perform field work in this region of Svalbard was granted by the Governor of Svalbard (RIS ID 5155, ref: 2012/00753–11 a.512). We thank Marthe Gjerde, Willem van der Bilt, Torgeir Røthe, and Sædis Ólafsdóttir for assistance with field work and Marthe and Willem for discussions on the manuscript. We also thank two anonymous reviewers for their constructive comments. Funding was provided by the Svalbard Science Forum (AFG project no. 235919) as well as the Norwegian Research Council via the SHIFTS (210004) project. We thank Eivind Storen and Jordan Donn Holl for laboratory assistance at the University of Bergen, and Nicole DeRoberts for laboratory assistance at Lamont Doherty Earth Observatory.

## References

Aagaard-Sørensen, S., Husum, K., Hald, M., Marchitto, T., Godtliebsen, F., 2014. Sub sea surface temperatures in the Polar North Atlantic during the Holocene: planktic foraminiferal Mg/Ca temperature reconstructions. *Holocene* 24, 93–103.

Alley, R.B., Mayewski, P.A., Sowers, T., Stuiver, M., Taylor, K.C., Clark, P.U., 1997. Holocene climatic instability: a prominent, widespread event 8200 yr ago. *Geology* 25, 483. [http://dx.doi.org/10.1130/0091-7613\(1997\)025<0483:HCAI>2.3.CO;2](http://dx.doi.org/10.1130/0091-7613(1997)025<0483:HCAI>2.3.CO;2).

Antoniades, D., 2008. *Diatoms of North America: the Freshwater Floras of Prince Patrick, Ellef Ringnes and Northern Ellesmere Islands from the Canadian Arctic Archipelago*.

Bakke, J., Trachsel, M., Kvisvik, B.C., Nesje, A., Lyså, A., 2013. Numerical analyses of a multi-proxy data set from a distal glacier-fed lake, Sørsendalsvatn, western Norway. *Quat. Sci. Rev.* 73, 182–195. <http://dx.doi.org/10.1016/j.quascirev.2013.05.003>.

Balascio, N.L., D'Andrea, W.J., Bradley, R.S., 2015. Glacier response to North Atlantic climate variability during the Holocene. *Clim. Past* 11, 1587–1598. <http://dx.doi.org/10.5194/cp-11-1587-2015>.

Balascio, N.L., D'Andrea, W.J., Gjerde, M., Bakke, J., Bradley, R.S., 2017. Leaf wax hydrogen isotope reconstruction of hydroclimate changes during the Holocene on Amsterdamøya, Svalbard. *Quat. Sci. Rev.* <http://dx.doi.org/10.1016/j.quascirev.2016.11.036> (in press).

Belt, S.T., Massé, G., Rowland, S.J., Poulin, M., Michel, C., LeBlanc, B., 2007. A novel chemical fossil of palaeo sea ice: IP25. *Org. Geochem.* 38, 16–27. <http://dx.doi.org/10.1016/j.orggeochem.2006.09.013>.

Berben, S.M.P., Husum, K., Cabedo-Sanz, P., Belt, S.T., 2014. Holocene sub-centennial evolution of Atlantic water inflow and sea ice distribution in the western Barents Sea. *Clim. Past* 10, 181–198. <http://dx.doi.org/10.5194/cp-10-181-2014>.

Birks, H.J.B., Jones, V.J., Rose, N.L., 2004. Recent environmental change and atmospheric contamination on Svalbard as recorded in lake sediments—synthesis and general conclusions. *J. Paleolimnol.* 31, 531–546.

Blaauw, M., 2010. Methods and code for “classical” age-modelling of radiocarbon sequences. *Quat. Geochronol.* 5, 512–518. <http://dx.doi.org/10.1016/j.quageo.2010.01.002>.

Blake, W., 2006. Occurrence of the *Mytilus edulis* complex on Nordaustlandet, Svalbard: radiocarbon ages and climatic implications. *Polar Res.* 25, 123–137.

Bond, G., 2001. Persistent solar influence on North Atlantic climate during the Holocene. *Science* 294, 2130–2136. <http://dx.doi.org/10.1126/science.1065680>.

Briner, J.P., McKay, N.P., Axford, Y., Bennike, O., Bradley, R.S., de Vernal, A., Fisher, D., Francus, P., Fréchette, B., Gajewski, K., Jennings, A., Kaufman, D.S., Miller, G., Rouston, C., Wagner, B., 2016. Holocene climate change in Arctic Canada and Greenland. *Quat. Sci. Rev.* 147, 340–364. <http://dx.doi.org/10.1016/j.quascirev.2016.02.010>.

Cabedo-Sanz, P., Belt, S.T., Jennings, A.E., Andrews, J.T., Geirsdóttir, Á., 2016. Variability in drift ice export from the Arctic Ocean to the North Icelandic Shelf over the last 8000 years: a multi-proxy evaluation. *Quat. Sci. Rev.* 146, 99–115. <http://dx.doi.org/10.1016/j.quascirev.2016.06.012>.

Callaghan, T.V., Bergholm, F., Christensen, T.R., Jonasson, C., Kokfelt, U., Johansson, M., 2010. A new climate era in the sub-Arctic: accelerating climate changes and multiple impacts: CHANGING CLIMATE IN THE SUB-ARCTIC. *Geophys. Res. Lett.* 37 <http://dx.doi.org/10.1029/2009GL042064> n/a-n/a.

Castañeda, I.S., Smith, L.M., Kristjánsdóttir, G.B., Andrews, J.T., 2004. Temporal changes in Holocene 180 records from the northwest and central North Iceland Shelf. *J. Quat. Sci.* 19, 321–334. <http://dx.doi.org/10.1002/jqs.841>.

D'Andrea, W.J., Vaillencourt, D.A., Balascio, N.L., Werner, A., Roof, S.R., Retelle, M., Bradley, R.S., 2012. Mild Little Ice Age and unprecedented recent warmth in an 1800 year lake sediment record from Svalbard. *Geology* 40, 1007–1010. <http://dx.doi.org/10.1130/G33365.1>.

Dean, W.E., 1974. Determination of carbonate and organic matter in calcareous sediments and sedimentary rocks by loss on ignition: comparison with other methods. *J. Sediment. Res.* 44.

Ebbesen, H., Hald, M., Eplet, T.H., 2007. Lateglacial and early Holocene climatic oscillations on the western Svalbard margin, European Arctic. *Quat. Sci. Rev.* 26, 1999–2011. <http://dx.doi.org/10.1016/j.quascirev.2006.07.020>.

Førland, E.J., Benestad, R., Hanssen-Bauer, I., Haugen, J.E., Skaugen, T.E., 2011. Temperature and precipitation development at svalbard 1900–2100. *Adv. Meteorol.* 2011, 1–14. <http://dx.doi.org/10.1155/2011/893790>.

Forman, S.L., 1990. Post-glacial relative sea-level history of northwestern Spitsbergen. *Svalbard. Geol. Soc. Am. Bull.* 102, 1580–1590.

Forwick, M., Vorren, T.O., 2009. Late Weichselian and Holocene sedimentary environments and ice rafting in Isfjorden, Spitsbergen. *Palaeogeogr. Palaeoclimatol. Palaeoecol.* 280, 258–274. <http://dx.doi.org/10.1016/j.palaeo.2009.06.026>.

Funder, S., Goosse, H., Jepsen, H., Kaas, E., Kjaer, K.H., Korsgaard, N.J., Larsen, N.K., Linderson, H., Lysa, A., Møller, P., Olsen, J., Willerslev, E., 2011. A 10,000-year record of Arctic ocean sea-ice variability—view from the beach. *Science* 333, 747–750. <http://dx.doi.org/10.1126/science.1202760>.

Gjermundsen, E.F., Briner, J.P., Akçar, N., Salvigsen, O., Kubik, P., Gantert, N., Hormes, A., 2013. Late Weichselian local ice dome configuration and chronology in Northwestern Svalbard: early thinning, late retreat. *Quat. Sci. Rev.* 72, 112–127. <http://dx.doi.org/10.1016/j.quascirev.2013.04.006>.

Gjerde, M., Bakke, J., D'Andrea, W.J., Balascio, N.L., Bradley, R., Vasskog, K., Ólafsdóttir, S., Røthe, T., Perren, B.B., Hormes, A., 2017. Holocene multi-proxy environmental reconstruction from Lake Hakluytvatnet, Amsterdamøya island, Svalbard (79.5°N). *Quat. Sci. Rev.* <http://dx.doi.org/10.1016/j.quascirev.2017.02.017> (in press).

Hald, M., Andersson, C., Ebbesen, H., Jansen, E., Klitgaard-Kristensen, D., Risebrobakken, B., Salomonsen, G.R., Sarnthein, M., Sejrup, H.P., Telford, R.J., 2007. Variations in temperature and extent of atlantic water in the northern North atlantic during the Holocene. *Quat. Sci. Rev.* 26, 3423–3440. <http://dx.doi.org/10.1016/j.quascirev.2007.10.005>.

Hald, M., Ebbesen, H., Forwick, M., Godtliebsen, F., Khomenko, L., Korsun, S., Ringstad Olsen, L., Vorren, T.O., 2004. Holocene paleoceanography and glacial history of the West Spitsbergen area, Euro-Arctic margin. *Quat. Sci. Rev.* 23, 2075–2088. <http://dx.doi.org/10.1016/j.quascirev.2004.08.006>.

Hammarlund, D., 1993. A distinct  $\delta^{13}\text{C}$  decline in organic lake sediments at the Pleistocene-Holocene transition in southern Sweden. *Boreas* 22, 236–243.

Heiri, O., Lotter, A.F., Lemcke, G., 2001. Loss on ignition as a method for estimating organic and carbonate content in sediments: reproducibility and comparability

of results. *J. Paleolimnol.* 25, 101–110.

Hjelle, A., Ohta, Y., 1974. Contribution to the geology of north western Spitsbergen. *Nor. Polarinst. Skr.* 158, 1–107.

Hoogakker, B.A.A., Chapman, M.R., McCave, I.N., Hillaire-Marcel, C., Ellison, C.R.W., Hall, I.R., Telford, R.J., 2011. Dynamics of North atlantic deep water masses during the Holocene: HOLOCENE N atlantic deep water dynamics. *Paleoceanography* 26. <http://dx.doi.org/10.1029/2011PA002155>.

Hormes, A., Gjermundsen, E.F., Rasmussen, T.L., 2013. From mountain top to the deep sea – deglaciation in 4D of the northwestern Barents Sea ice sheet. *Quat. Sci. Rev.* 75, 78–99. <http://dx.doi.org/10.1016/j.quascirev.2013.04.009>.

Humlum, O., Elberling, B., Hormes, A., Fjordheim, K., Hansen, O.H., Heinemeier, J., 2005. Late-Holocene glacier growth in Svalbard, documented by subglacial relict vegetation and living soil microbes. *Holocene* 15, 396–407.

Ingólfsson, O., Landvik, J.Y., 2013. The Svalbard–Barents Sea ice-sheet – historical, current and future perspectives. *Quat. Sci. Rev.* 64, 33–60. <http://dx.doi.org/10.1016/j.quascirev.2012.11.034>.

Johnsen, S.J., Dahl-Jensen, D., Gundestrup, N., Steffensen, J.P., Clausen, H.B., Miller, H., Masson-Delmotte, V., Sveinbjørnsdóttir, A.E., White, J., 2001. Oxygen isotope and palaeotemperature records from six Greenland ice-core stations: camp Century, Dye-3, GRIP, GISP2, Renland and NorthGRIP. *J. Quat. Sci.* 16, 299–307. <http://dx.doi.org/10.1002/jqs.622>.

Kaplan, M.R., Wolfe, A.P., 2006. Spatial and temporal variability of Holocene temperature in the North Atlantic region. *Quat. Res.* 65, 223–231. <http://dx.doi.org/10.1016/j.yqres.2005.08.020>.

Kaufman, D.S., Ager, T.A., Anderson, N.J., Anderson, P.M., Andrews, J.T., Bartlein, P.J., Brubaker, L.B., Coats, L.L., Cwynar, L.C., Duvall, M.L., others, 2004. Holocene thermal maximum in the western Arctic (0–180° W). *Quat. Sci. Rev.* 23, 529–560.

Knudsen, K., Jiang, H., Jansen, E., Eiriksson, J., Heinemeier, J., Seidenkrantz, M.-S., 2004. Environmental changes off North Iceland during the deglaciation and the Holocene: foraminifera, diatoms and stable isotopes. *Mar. Micropaleontol.* 50, 273–305. [http://dx.doi.org/10.1016/S0377-8398\(03\)00075-6](http://dx.doi.org/10.1016/S0377-8398(03)00075-6).

Kubischa, F., Knudsen, K.L., Ojala, A.E., Salonen, V.-P., 2011. Holocene benthic foraminiferal record from a high-arctic fjord, nordaustlandet, Svalbard. *Geogr. Ann. Ser. Phys. Geogr.* 93, 227–242.

Landvik, J.Y., Bondevik, S., Elverhøi, A., Fjeldskaar, W., Mangerud, J., Salvigsen, O., Siegert, M.J., Svendsen, J.-I., Vorren, T.O., 1998. The last glacial maximum of Svalbard and the Barents Sea area: ice sheet extent and configuration. *Quat. Sci. Rev.* 17, 43–75.

Landvik, J.Y., Brook, E.J., Gualtieri, L., Raisbeck, G., Salvigsen, O., Yiou, F., 2003. Northwest Svalbard during the last glaciation: ice-free areas existed. *Geology* 31, 905–908.

Laskar, J., Robutel, P., Joutel, F., Gastineau, M., Correia, A.C.M., Levrard, B., others, 2004. A long-term numerical solution for the insolation quantities of the Earth. *Astron. Astrophys.* 428, 261–285.

Mayewski, P.A., Rohling, E.E., Curt Stager, J., Karlén, W., Maasch, K.A., David Meeker, L., Meyerson, E.A., Gasse, F., van Kreveld, S., Holmgren, K., Lee-Thorp, J., Rosqvist, G., Rack, F., Staubwasser, M., Schneider, R.R., Steig, E.J., 2004. Holocene climate variability. *Quat. Res.* 62, 243–255. <http://dx.doi.org/10.1016/j.yqres.2004.07.001>.

Meyers, P.A., 1997. Organic geochemical proxies of paleoceanographic, paleolimnologic, and paleoclimatic processes. *Org. Geochem.* 27, 213–250.

Miller, G.H., Brigham-Grette, J., Alley, R.B., Anderson, L., Bauch, H.A., Douglas, M.S.V., Edwards, M.E., Elias, S.A., Finney, B.P., Fitzpatrick, J.J., Funder, S.V., Herbert, T.D., Hinzman, L.D., Kaufman, D.S., MacDonald, G.M., Polyak, L., Robock, A., Serreze, M.C., Smol, J.P., Spielhagen, R., White, J.W.C., Wolfe, A.P., Wolff, E.W., 2010. Temperature and precipitation history of the Arctic. *Quat. Sci. Rev.* 29, 1679–1715. <http://dx.doi.org/10.1016/j.quascirev.2010.03.001>.

Mooszen, H., Bendle, J., Seki, O., Quillmann, U., Kawamura, K., 2015. North Atlantic Holocene climate evolution recorded by high-resolution terrestrial and marine biomarker records. *Quat. Sci. Rev.* 129, 111–127. <http://dx.doi.org/10.1016/j.quascirev.2015.10.013>.

Müller, J., Massé, G., Stein, R., Belt, S., 2009. Variability of sea-ice conditions in the Fram Strait over the past 30,000 years. *Nat. Geosci.* 2, 772–776.

Müller, J., Werner, K., Stein, R., Fahl, K., Moros, M., Jansen, E., 2012. Holocene cooling culminates in sea ice oscillations in Fram Strait. *Quat. Sci. Rev.* 47, 1–14. <http://dx.doi.org/10.1016/j.quascirev.2012.04.024>.

Ohta, Y., Hjelle, A., Dallmann, W.K. (Eds.), 2007. *Geological Map Svalbard 1:100 000, Sheet A4G, Vasahalvøya*. Norsk Polarinstitutt Temakart Nr. 40.

Perren, B.B., Massa, C., Bichet, V., Gauthier, É., Mathieu, O., Petit, C., Richard, H., 2012. A paleoecological perspective on 1450 years of human impacts from a lake in southern Greenland. *Holocene* 22, 1025–1034.

R Development Core Team, 2012. R: A Language and Environment for Statistical Computing. R Foundation for Statistical Computing, Vienna, Austria.

Rasmussen, T.L., Forwick, M., Mackensen, A., 2013. Reprint of: reconstruction of inflow of atlantic water to isfjorden, svalbard during the Holocene: correlation to climate and seasonality. *Mar. Micropaleontol.* 99, 18–28. <http://dx.doi.org/10.1016/j.marmicro.2013.03.011>.

Rasmussen, T.L., Thomsen, E., Skirbekk, K., Ślubowska-Woldengen, M., Klitgaard Kristensen, D., Koç, N., 2014. Spatial and temporal distribution of Holocene temperature maxima in the northern Nordic seas: interplay of Atlantic-, Arctic- and polar water masses. *Quat. Sci. Rev.* 92, 280–291. <http://dx.doi.org/10.1016/j.quascirev.2013.10.034>.

Reimer, P.J., Bard, E., Bayliss, A., Beck, J.W., Blackwell, P.G., Ramsey, C.B., Buck, C.E., Cheng, H., Edwards, R.L., Friedrich, M., others, 2013. IntCal13 and Marine13 radiocarbon age calibration curves 0–50,000 years cal BP. *Radiocarbon* 55, 1869–1887.

Renberg, I., 1990. A procedure for preparing large sets of diatom slides from sediment cores. *J. Paleolimnol.* 4, 87–90.

Reusche, M., Winsor, K., Carlson, A.E., Marcott, S.A., Rood, D.H., Novak, A., Roof, S., Retelle, M., Werner, A., Caffee, M., Clark, P.J., 2014. 10Be surface exposure ages on the late-Pleistocene and Holocene history of Linnebreen on Svalbard. *Quat. Sci. Rev.* 89, 5–12. <http://dx.doi.org/10.1016/j.quascirev.2014.01.017>.

Risebrobakken, B., Dokken, T., Smedsrød, L.H., Andersson, C., Jansen, E., Moros, M., Ivanova, E.V., 2011. Early Holocene temperature variability in the Nordic Seas: the role of oceanic heat advection versus changes in orbital forcing: early holocene advection vs. insolation. *Paleoceanography* 26. <http://dx.doi.org/10.1029/2011PA002117>.

Rohling, E.J., Pálike, H., 2005. Centennial-scale climate cooling with a sudden cold event around 8,200 years ago. *Nature* 434, 975–979.

Røthe, T.O., Bakke, J., Vasskog, K., Gjerde, M., D'Andrea, W.J., Bradley, R.S., 2015. Arctic Holocene glacier fluctuations reconstructed from lake sediments at Mitrahalvøya, Spitsb. *Quat. Sci. Rev.* 109, 111–125. <http://dx.doi.org/10.1016/j.quascirev.2014.11.017>.

Salvigsen, O., 2002. Radiocarbon-dated *Mytilus edulis* and *Modiolus modiolus* from northern svalbard: climatic implications. *Nor. Geogr. Tidsskr. - Nor. J. Geogr.* 56, 56–61. <http://dx.doi.org/10.1080/002919502760056350>.

Sarnthein, M., Kreveld, S., Erlenkeuser, H., Grootes, P., Kucera, M., Pflaumann, U., Schulz, M., 2003. Centennial-to-millennial-scale periodicities of Holocene climate and sediment injections off the western Barents shelf, 75° N. *Boreas* 32, 447–461.

Sejrup, H.P., Seppä, H., McKay, N.P., Kaufman, D.S., Geirsdóttir, Á., de Vernal, A., Renssen, H., Husum, K., Jennings, A., Andrews, J.T., 2016. North Atlantic–Fennoscandian Holocene climate trends and mechanisms. *Quat. Sci. Rev.* 147, 365–378. <http://dx.doi.org/10.1016/j.quascirev.2016.06.005>.

Serreze, M.C., Barry, R.G., 2011. Processes and impacts of Arctic amplification: a research synthesis. *Glob. Planet. Change* 77, 85–96. <http://dx.doi.org/10.1016/j.gloplacha.2011.03.004>.

Skirbekk, K., Kristensen, D.K., Rasmussen, T.L., Koç, N., Forwick, M., 2010. Holocene climate variations at the entrance to a warm Arctic fjord: evidence from Kongsfjorden trough, Svalbard. *Geol. Soc. Lond. Spec. Publ.* 344, 289–304.

Ślubowska, M.A., Koç, N., Rasmussen, T.L., Klitgaard-Kristensen, D., 2005. Changes in the flow of Atlantic water into the Arctic Ocean since the last deglaciation: evidence from the northern Svalbard continental margin, 80°N: ATLANTIC WATER INFLOW INTO ARCTIC OCEAN. *Paleoceanography* 20. <http://dx.doi.org/10.1029/2005PA001141> n/a–n/a.

Ślubowska, M.A., Rasmussen, T.L., Koç, N., Klitgaard-Kristensen, D., Nilsen, F., Solheim, A., 2007. Advection of Atlantic Water to the western and northern Svalbard shelf since 17,500 cal yr BP. *Quat. Sci. Rev.* 26, 463–478.

Snyder, J.A., Werner, A., Miller, G.H., 2000. Holocene cirque glacier activity in western Spitsbergen, Svalbard: sediment records from proglacial Linnévatnet. *Holocene* 10, 555–563.

Stocker, T.F., Qin, D., Plattner, G.-K., Tignor, M., Allen, S.K., Boschung, J., Nauels, A., Xia, Y., Bex, V., Midgley, P.M., 2013. Climate Change 2013: the Physical Science Basis. Intergov. Panel Clim. Change Work. Group Contrib. IPCC Fifth Assess. Rep. AR5Cambridge Univ Press, N. Y.

Svendsen, J.I., Mangerud, J., 1997. Holocene glacial and climatic variations on Spitsbergen, Svalbard. *Holocene* 7, 45–57.

Thomas, E.R., Wolff, E.W., Mulvaney, R., Steffensen, J.P., Johnsen, S.J., Arrowsmith, C., White, J.W.C., Vaughn, B., Popp, T., 2007. The 8.2ka event from Greenland ice cores. *Quat. Sci. Rev.* 26, 70–81. <http://dx.doi.org/10.1016/j.quascirev.2006.07.017>.

van der Bilt, W.G.M., Bakke, J., Vasskog, K., D'Andrea, W.J., Bradley, R.S., Ólafsdóttir, S., 2015. Reconstruction of glacier variability from lake sediments reveals dynamic Holocene climate in Svalbard. *Quat. Sci. Rev.* 126, 201–218. <http://dx.doi.org/10.1016/j.quascirev.2015.09.003>.

van der Bilt, W.G.M., D'Andrea, W.J., Bakke, J., Balascio, N.L., Werner, J.P., Gjerde, M., Bradley, R.S., 2016. Alkenone-based reconstructions reveal four-phase Holocene temperature evolution for High Arctic Svalbard. *Quat. Sci. Rev.* <http://dx.doi.org/10.1016/j.quascirev.2016.10.006>.

Velle, G., Kongshavn, K., Birks, H.J.B., 2011. Minimizing the edge-effect in environmental reconstructions by trimming the calibration set: chironomid-inferred temperatures from Spitsbergen. *Holocene* 21, 417–430. <http://dx.doi.org/10.1177/0959683610385723>.

Werner, K., Müller, J., Husum, K., Spielhagen, R.F., Kandiano, E.S., Polyak, L., 2015. Holocene sea subsurface and surface water masses in the Fram Strait – comparisons of temperature and sea-ice reconstructions. *Quat. Sci. Rev.* <http://dx.doi.org/10.1016/j.quascirev.2015.09.007>.

Werner, K., Spielhagen, R.F., Bauch, D., Hass, H.C., Kandiano, E., 2013. Atlantic Water advection versus sea-ice advances in the eastern Fram Strait during the last 9 ka: multiproxy evidence for a two-phase Holocene: holocene in eastern fram strait. *Paleoceanography* 28, 283–295. <http://dx.doi.org/10.1002/palo.20028>.

Wojtal, A.Z., Ognjanova-Rumenova, N., Wetzel, C.E., Hinz, F., Piatek, J., Kapetanovic, T., Ector, L., Buczko, K., 2014. Diversity of the genus *Genkalia* (Bacillariophyta) in boreal and mountain lakes-taxonomy, distribution and ecology. *Fottea* 14, 225–239.